Final Report

Polarization Diversity Active Imaging:
Mueller Matrix Imaging Polarimetry of Spheres and Cones
Estimation of the Refractive Index from the Polarization Signatures

submitted for:
Contract #DAFG60-96-C-0134 mod.2
Proposal #97-297

Covering:
July, 1997 - December, 1997

Scientific Personnel
Russell A. Chipman, Associate Professor of Physics
Pierre-Yves Gerligand, Research Associate
Matthew H. Smith, Research Scientist

Polarization and Lens Design Laboratory
Department of Physics
Optics Bldg. 318
The University of Alabama in Huntsville
Huntsville, AL 35899

telephone: (205)890-6417 ext.318
Facsimile: (205)890-6873
Email: chipmanr@email.uah.edu

Contracting Office:
Dr. Ralph Kelly
Air Force Office of Scientific Research
Bolling Air Force Base
Washington, DC

REPORT DOCUMENTATION PAGE

Form Approved
OMB NO. 0704-0188

1. AGENCY USE ONLY *(Leave blank)*	2. REPORT DATE	3. REPORT TYPE AND DATES COVERED
	January 1998	Final Report 4/97 thru 12/97

4. TITLE AND SUBTITLE
Polarization Diversity Active Imaging: Mueller Matrix Imaging Polarimetry of Sphers and Cones Estimation of the Refrative Index

5. FUNDING NUMBERS
DASG60-96-C-0134 Mod. 2

6. AUTHOR(S)
Russell A. Chipman, Pierre-Yves Gerligand and Matthew Smith

7. PERFORMING ORGANIZATION NAMES(S) AND ADDRESS(ES)
University of Alabama in Huntsville
301 Sparkman Drive, OB318
Huntsville, AL 35899

8. PERFORMING ORGANIZATION REPORT NUMBER

9. SPONSORING / MONITORING AGENCY NAME(S) AND ADDRESS(ES)

10. SPONSORING / MONITORING AGENCY REPORT NUMBER

11. SUPPLEMENTARY NOTES

12a. DISTRIBUTION / AVAILABILITY STATEMENT

Approved for public release; distribution unlimited.

19980305 062

13. ABSTRACT *(Maximum 200 words)*

A previous study presented interesting data indicating the ability of the Polarization Diversity Active Imaging technique (PDAI) to measure polarization signatures of objects of simple shape (conical and spherical objects). Polarimetric signatures of such objects are obtained by applying a powerful decomposition technique, previously developed under earlier AFOSR contract. A complete description of the object in then obtained. Such decomposition can be used for detection, discrimination and classification of targets. (70)

This second phase has extended the study of the dynamic behavior of one of the previous targets (cone used as a re-entry vehicle model). By then rotating that sample target to make polarization movie, the evolution of the decomposed polarization signature can then be fully examined. The analysis performed for each position finally provides the dynamic behaviors of the target depending on either its orientation or the position of the detection system.

The second goal of this phase was the development of a method for estimating the refractive index of a target from its Mueller matrix image. Our investigations show that the refractive index can be estimated either by using data resulting from the polar decomposition method or from the Mueller matrix image of the object after different steps of data processing. Such parameter is essential in order to progress in the understanding of these polarized light/material interactions.

14. SUBJECT TERMS	15. NUMBER IF PAGES
	/
	16. PRICE CODE

Final Report

Polarization Diversity Active Imaging:
Mueller Matrix Imaging Polarimetry of Spheres and Cones
Estimation of the Refractive Index from the Polarization Signatures

submitted for:
Contract #DAFG60-96-C-0134 mod.2
Proposal #97-297

Covering:
July, 1997 - December, 1997

Scientific Personnel
Russell A. Chipman, Associate Professor of Physics
Pierre-Yves Gerligand, Research Associate
Matthew H. Smith, Research Scientist

Polarization and Lens Design Laboratory
Department of Physics
Optics Bldg. 318
The University of Alabama in Huntsville
Huntsville, AL 35899

telephone: (205)890-6417 ext.318
Facsimile: (205)890-6873
Email: chipmanr@email.uah.edu

Contracting Office:
Dr. Ralph Kelly
Air Force Office of Scientific Research
Bolling Air Force Base
Washington, DC

Table of Contents

Table of Figures

1. Summary

This final report documents the second phase of the Polarization Diversity Active Imaging (PDAI) research program performed at the Physics department of the University of Alabama in Huntsville (UAH).

Polarization Diversity Active Imaging illuminates a scene or target with a sequence of polarization states and then measures images of the polarization states scattered from the scene or target. These polarization images are then analyzed to provide additional details in the optical signature of objects by quantifying the object interaction with polarized light.

The first phase of this research program has investigated the possibility to discriminate and identify targets from their polarization signatures. Measurements were taken on two types of targets (spherical and conical targets) by using the Mueller Matrix Imaging Polarimeter (MMIP, see Annexe A). The polarization characteristics were deduced from the polar decomposition method developed by S.Y. Lu and R.A. Chipman [1]. The different data sets obtained have showed an existing correlation between the orientation and the shape of the object and its polarization signature. During the second phase, we have extended our research in order to study the behavior of one of the previous target (brass (gold-toned) cone with rounded tip used as a re-entry vehicle model) for different positions of the target and positions of the detection system (polarization analyzer). The analysis performed for each position finally provides the dynamic behaviors of the target depending on either its orientation or the position of the detection system. Both cases lead to a complete description of the target through its polarization signature expressed in terms of depolarization, diattenuation and retardance properties.

The second goal of the phase II was the development of an estimation method for determining the refractive index of a target from its Mueller matrix image. The method has been

applied on the four previous spherical targets, described in the precedent reports, and on four other objects (metal and glass plates). Our investigations show that the refractive index can be estimated either by using data resulting from the polar decomposition method or from the Mueller matrix image of the object after different steps of data processing. Both methods lead to the same results and require the resolution of the fundamental equation of Ellipsometry.

This final report documents the following accomplishments performed during the second phase under our AFOSR contract:

- Measured the Mueller matrix images of the brass cone under different orientations of the target and the polarization analyzer of the MMIP
- Calculated polarization signatures of the brass cone
  - magnitude and orientation of the retardance
  - magnitude and orientation of the diattenuation
  - polarizance and depolarization index
  - horizontal-to-vertical and left-to-right crosstalks
- Upgraded the Mueller Matrix Imaging Polarimeter with a new 16 bits CCD camera
- Developed technique to estimate the refractive index from a Mueller matrix image
- Calculated the refractive index for our spherical targets
- Calculated the refractive index for four other objects

Two important remarks must be mentioned from these different investigations:

- *Some of the polarization characteristics (diattenuation and retardance) become difficultly exploitable* when the orientation of the object or the position of the polarization analyzer varies. Polarization signatures are then too noisy to recognize either the shape or the orientation of the object.

- The refractive index can not be estimated from the previous spherical targets. The small value of the angle of incidence does not permit a good estimation. However, *refractive indices deduced from the other objects (estimation of the refractive index from a plane surface) are in agreement with values given in the literature*.

However, further investigations are necessary to comfort these results and to complete this work. The extension of the study using some very specific samples (calibrated in roughness and machined in only one material for example) will improve a lot the understanding of the polarization phenomena.

2. Movie samples obtained from the PDAI technique

First investigations concerning the polarization signatures of spherical and conical targets were obtained only for a given orientation of the object under analyzed. The bistatic angle used for these characterizations was about 10 degrees. Such a configuration gives only a static description of the polarization signature of any object and can not give an estimation of how the signature will be for an other position of the target or the detection system. During this second phase we have extended the previous analyzes corresponding to a "static configuration" to a "dynamic configuration". This analysis was performed by using one of the targets for which the signature was well defined: the brass (gold-toned) cone with rounded tip. Two configurations were applied for this analysis. First, the object was rotated and the polarization generator and polarization analyzer of the MMIP were maintained in the same position. Secondly, the orientation of the object was maintained and the position of the polarization analyzer was changed. Both methods give similar results and relatively well describe the polarimetric behavior of the object as function of its position.

2.1. Rotation of the target

The polarization signature of the brass cone was measured for different positions of the target. The value of the bistatic angle was 10 degrees. The light source was a HeNe laser emitting at 633 nm. The brass cone was rotated from 0 degree (cone perpendicular to the laser beam) to 180 degrees with a rotation step of 10 degrees as shown in Figure 1. For each position we have applied the polar decomposition onto the Mueller matrix images and observed the evolution of the following parameters:

- magnitude and orientation of the retardance
- magnitude and orientation of the diattenuation
- horizontal-to-vertical and left-to-right crosstalk
- polarizance and depolarization index

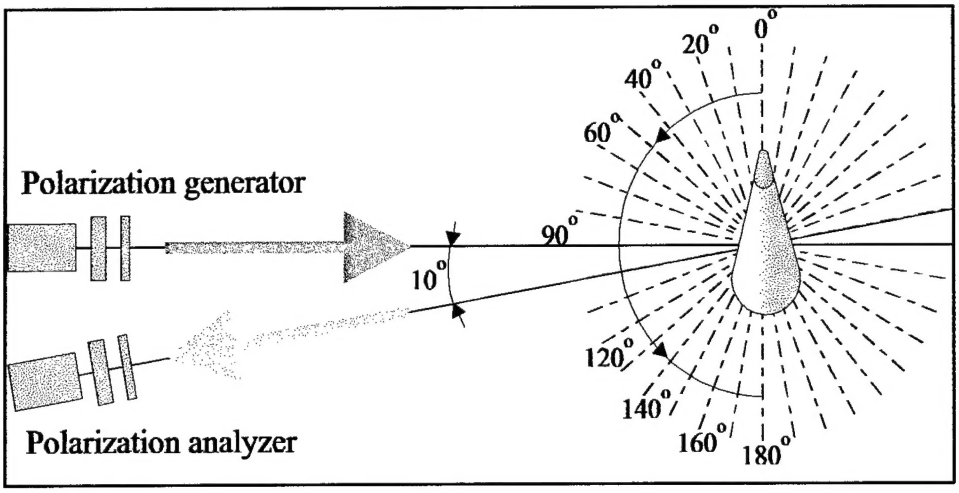

Figure 1: First geometry of test of the brass cone.

The following sets of images, presented on pages 9-12, have been extracted from a movie generated by using for each position the polarization signatures of the brass cone. They present the evolution of each parameter previously mentioned for six different positions of the targets from 0 degree to 150 degrees. Images were taken with a relatively large size (200 x 70 pixels) in order to have a very good definition.

As shown on Figure 3 which represents the magnitude and orientation of the retardance, the signature of the object is obvious whatever its position. The orientation of the retardance describes perfectly the shape of the object and its orientation. For example, the orientation of the object for the first two positions (0° and 30°) seems to be identical when we observe only the magnitude of the retardance. However, from the orientation we can deduce from the first image that the right extremity of the cone is closest to the polarization analyzer than the tip. On the second image the positions of the right extremity and the tip are inverted. Orientation and shape are a little more described by the line graphs on Figure 2 and on Appendix B.

From the orientation of the diattenuation (Figure 4),the orientation and the shape of the brass cone can be only estimated when the orientation of the target is ranged from 50 to 130 degrees. For

the other positions the magnitude of the diattenuation is very weak which leads for the orientation to a noisy pattern difficultly interpretable.

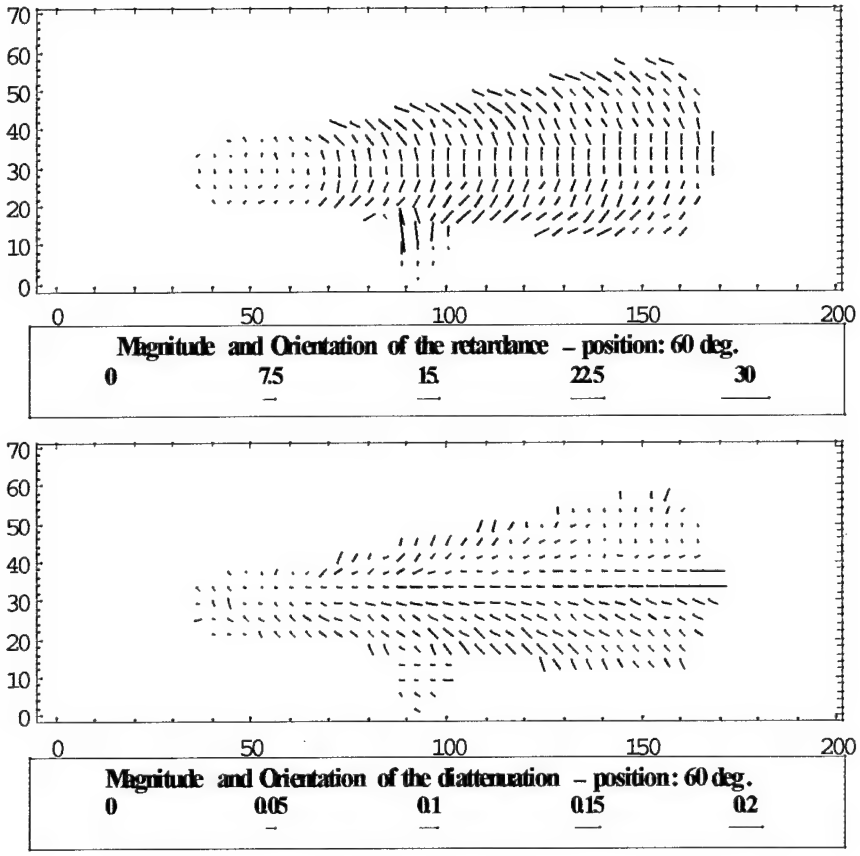

Figure 2: Retardance and diattenuation ligne graph images for position 60° .

Horizontal-to-vertical and left-to-right crosstalk images (Figure 5) have also some significant changes according to the position of the target. The first set of images (horizontal-to-vertical crosstalk images) gives much more details on the orientation and shape of the object than the second set.

Polarizance and depolarization index images (Figure 6) do not give so many details on the orientation and shape of the target. However, such parameters remain essential to estimate the polarizing and depolarizing power of the object.

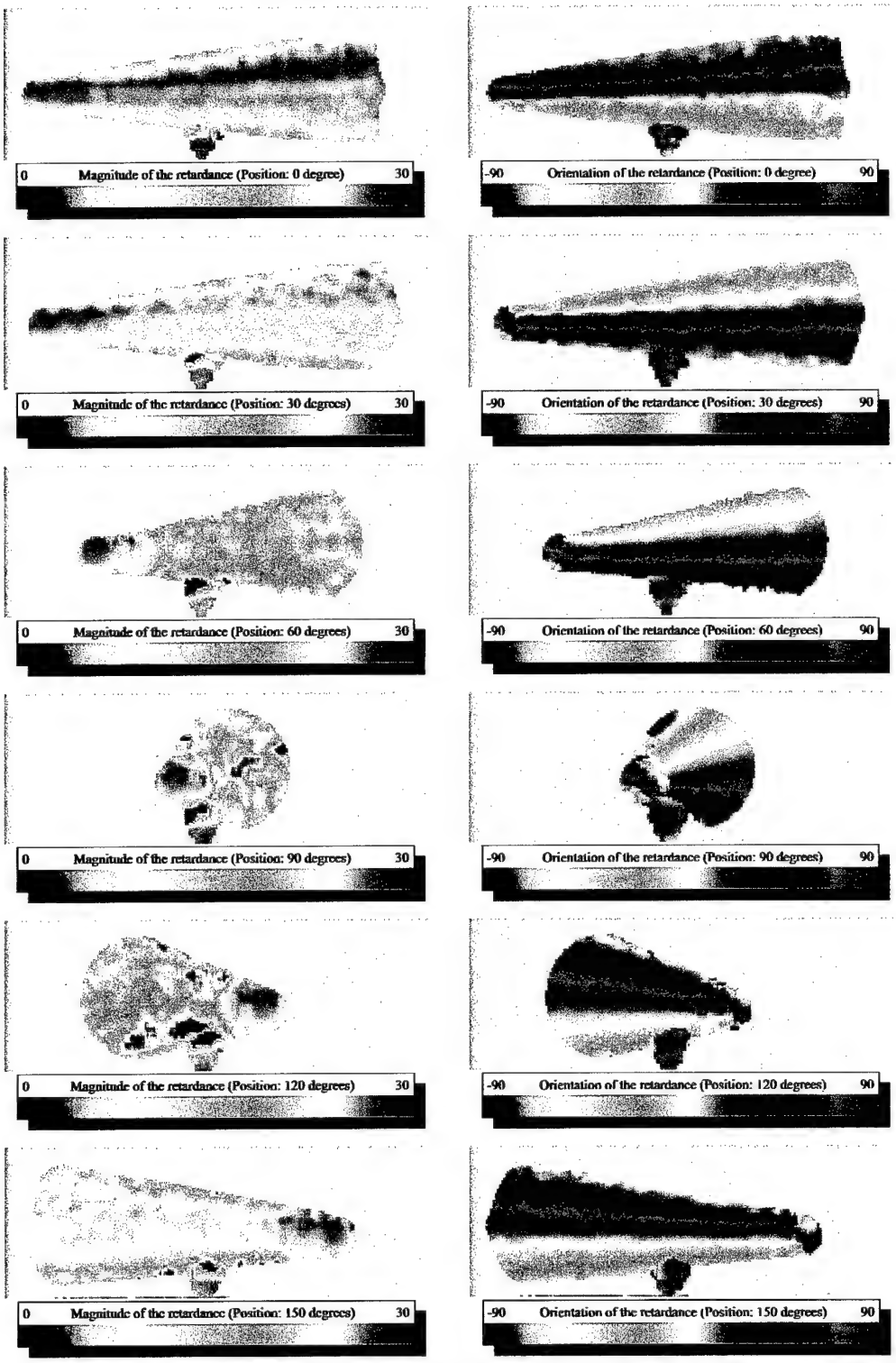

Figure 3: Magnitude and orientation images of the retardance for different orientations of the brass cone (0°, 30°, 60°, 90°, 120°, 150°).

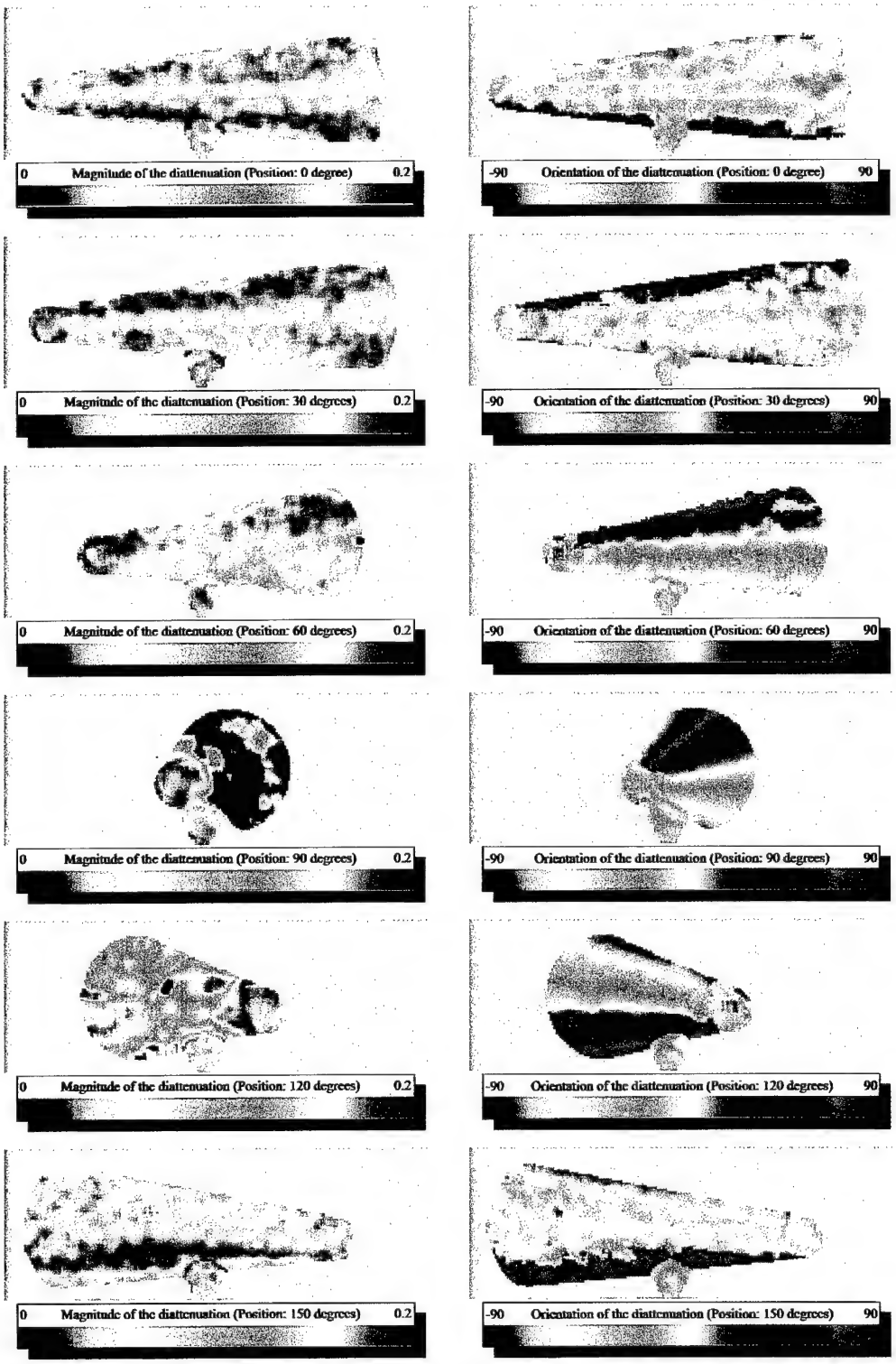

Figure 4: Magnitude and orientation images of the diattenuation for different orientations of the brass cone (0°, 30°, 60°, 90°, 120°, 150°).

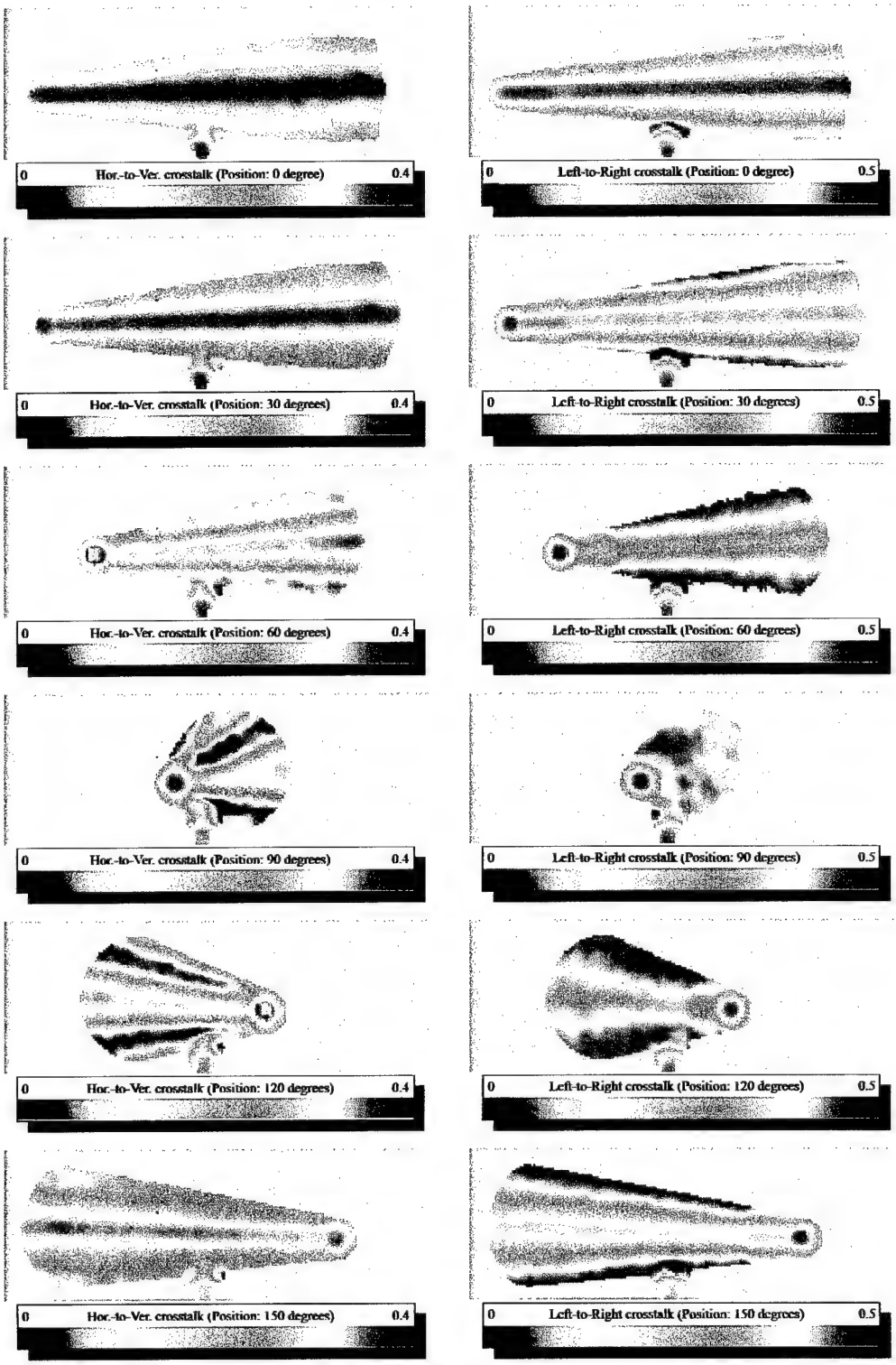

Figure 5: Horizontal-to-vertical and left-to-right crosstalk images for different orientations of the brass cone (0°, 30°, 60°, 90°, 120°, 150°).

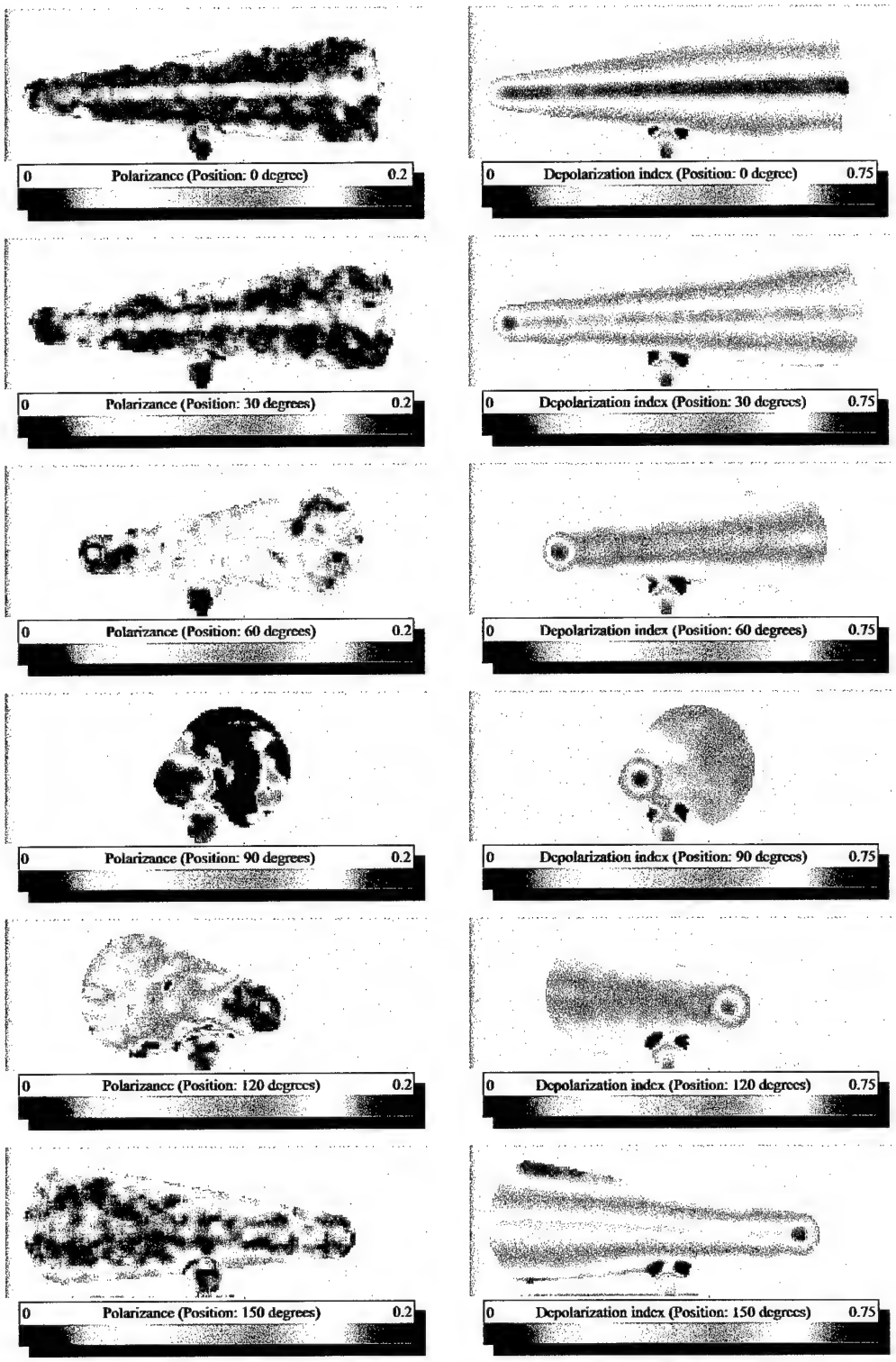

Figure 6: Polarizance and depolarization index images for different orientations of the brass cone (0°, 30°, 60°, 90°, 120°, 150°).

2.2. Rotation of the polarization analyzer

The initial position of the polarization analyzer corresponds to a bistatic angle of 15 degrees. The principal axis of the cone is 10 degrees off of the direction perpendicular to the propagation direction of the laser beam. Measurements were taken using a rotation step of 5 degrees for the polarization analyzer (Figure 7). Images have a smaller resolution (150 x 50) than the previous data sets in order to reduce the calculation time during the data reduction process.

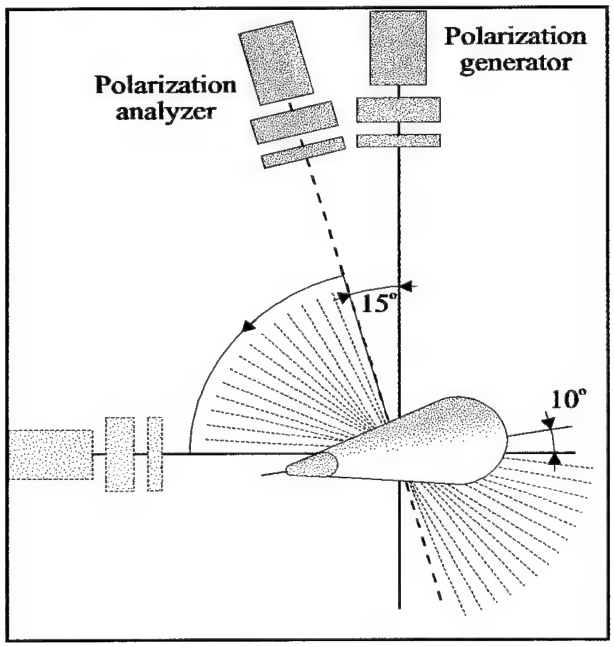

Figure 7: Second geometry of test of the brass cone.

The characteristics obtained from this configuration have not a so good resolution than the precedent sets but the dynamic behavior of each parameter confirms those previously found. Retardance, diattenuation, crosstalk and polarization images corresponding to this set are presented in Appendix C for six distinct positions of the polarization analyzer (15°, 30°, 45°, 60°, 75°, 90°).

3. Estimation of the refractive index from the Mueller matrix image

3.1 Introduction

Numerous studies have been conducted to understand the interactions of light with dielectric or conducting surfaces either in reflection or refraction (transmission). This behavior is expressed mathematically from a set of equations called Fresnel's equations. For an air/conducting interface Fresnel's equations for reflection are [2]:

$$r_P = \frac{n.\cos\theta_i - \cos\theta_r}{n.\cos\theta_i + \cos\theta_r} \quad (1a)$$

$$r_S = \frac{\cos\theta_i - n.\cos\theta_r}{\cos\theta_i + n.\cos\theta_r} \quad (1b)$$

where θ_i and θ_r are the angle of incidence and the angle of refraction respectively and n the refractive index of the medium. For conducting media, the refractive index becomes complex and has the form n (1 - ik) where n is the refractive index and k the extinction coefficient.

Although problems involving polarization in reflection and refraction are complex, they can be treated in a simple way by expressing the Fresnel's equations in the form of Stokes vectors and Mueller matrices. Both reflection and refraction lead to Mueller matrices which correspond to polarizing elements. Mueller matrices for reflection are directly expressed from the reflection coefficients which describe the amplitude and phase changes of the incident light after reflection onto the surface. The refractive index is then deduced by first determining the normalized reflection coefficient and by resolving the fundamental equation of Ellipsometry.

3.2. Mueller matrix for reflection

As the reflection of a light onto a surface results in a change of amplitude and phase of the incident fields, the reflection coefficients r_p and r_s can then be expressed in terms of these changes. If r_P and r_S are defined as:

$$r_P = \frac{R_P}{E_P} = \rho_P Exp[i.\phi_P] \tag{2a}$$

$$r_S = \frac{R_S}{E_S} = \rho_S Exp[i.\phi_S] \tag{2b}$$

where ρ_p and ρ_s represent the amplitude changes and ϕ_P and ϕ_S the phase changes of each component respectively, then, we can introduce a new parameter: the normalized reflection coefficient ρ defined by:

$$\rho = \frac{r_P}{r_S} = Tan\psi.Exp[i.\Delta] = \rho_0 Exp[i.\Delta] \tag{3}$$

with $$Tan\psi = \frac{R_P.E_S}{R_S.E_P} = \frac{\rho_P}{\rho_S}$$

and $$\Delta = \phi_S - \phi_P$$

The final expression of the Mueller matrix for reflection M_{ref} is obtained by formulating the equations of ellipsometry in terms of the ABCD matrix and the Stokes polarization parameters. M_{ref} is than expressed from the normalized reflection coefficient ρ as [3]:

$$M_{Ref} = M[m_{ij}] = \frac{\rho_S \rho_S^*}{2} \begin{bmatrix} 1+Tan^2\psi & 1-Tan^2\psi & 0 & 0 \\ 1-Tan^2\psi & 1+Tan^2\psi & 0 & 0 \\ 0 & 0 & 2.Tan\psi.cos\Delta & -2.Tan\psi.sin\Delta \\ 0 & 0 & 2.Tan\psi.sin\Delta & 2.Tan\psi.cos\Delta \end{bmatrix} \tag{4}$$

3.3. Determination of M_{ref} from an experimental Mueller matrix

Usually the Mueller matrix resulting from an experiment is given in an arbitrary coordinates system which does not correspond to the S-P coordinates system used to describe M_{ref}. Then different operations must be applied onto the experimental Mueller matrix in order to obtain M_{ref}.

First the experimental Mueller matrix M is deduced from the Mueller matrix image of the surface of the object by determining an average Mueller matrix in the specular direction. In this direction the angle of incidence is equal to half of the value of the bistatic angle. M is then decomposed, by applying the polar decomposition, to a product of three matrices (depolarization, retardance and diattenuation matrices) in order to extract the depolarizing component.

$$\mathbf{M} = \mathbf{M_P}.\mathbf{M_R}.\mathbf{M_D} \tag{5}$$

$$\mathbf{M_{Ref}}' = \mathbf{M_P}^{-1}.\mathbf{M} = \mathbf{M_R}.\mathbf{M_D} \tag{6}$$

When the depolarization has been extracted from the average Mueller matrix, M_{ref}' must be rotated by an angle θ to be expressed in the same coordinate system of M_{ref}.

$$\begin{aligned} \mathbf{M_{Ref}}' &= \mathbf{R}(2\theta).\mathbf{M_{Ref}}\mathbf{R}(-2\theta) \\ \mathbf{M_{Ref}} &= \mathbf{R}(-2\theta).\mathbf{M_{Ref}}'.\mathbf{R}(2\theta) \end{aligned} \tag{7}$$

We know, from the eigen-values equation, that if we apply any incident polarization state in one of the eigen-directions of an element, the emergent state will have the same polarization. The simplest way to determine θ is to define what incident linear polarization will emerge with a null ellipticity. The orientation of the incident linear polarization then gives the angle θ representing the orientation of one of the eigen-directions relative to the horizontal direction (reference). In general the Mueller matrix resulting from the product of two non-depolarizing Mueller matrices is

inhomogeneous. The matrix is homogeneous only if the first two matrices have their eigen-directions aligned. From both cases θ can be deduced by applying the technique previously described. From this assumption, θ is determined by resolving the following relationship:

Ellipticity $[M_{Ref}'.S(\theta)] = 0$ ($S(\theta)$: linear polarization state oriented at θ)

or

$$m_{30} + m_{31}.\cos(2\theta) + m_{32}.\sin(2\theta) = 0 \qquad (8)$$

The solutions of this equation then give the two eigen-directions of M_{ref}'. These solutions are:

$$\theta_{1,2} = \mathrm{ArcTan}\left[\frac{\pm\sqrt{m_{31}^2+m_{32}^2-m_{30}^2}-m_{32}}{m_{30}-m_{31}}\right] \qquad (9)$$

By applying one of these solutions in the equation (7), the form of the experimental Mueller matrix becomes the standard form of M_{ref} (equation (4)). The reflection coefficient can then be estimated after this transformation.

The inhomogeneity can be expressed in terms of the solutions θ_1 and θ_2 as:

$$\eta = \mathrm{Cos}(|\theta_1 - \theta_2|) \qquad 0 \le \eta \le 1 \qquad (10)$$

3.4. Estimation of the normalized reflection coefficient

By applying onto the Mueller matrix M_{ref} a horizontal linear polarization and a vertical linear polarization respectively, we obtain the magnitude of the normalized reflection coefficient ρ:

$$\rho_S = \sqrt{\frac{S_{0H}+S_{1H}}{2}} \qquad \rho_P = \sqrt{\frac{S_{0V}-S_{1V}}{2}} \qquad (11a)$$

$$\rho_0 = \frac{\rho_P}{\rho_S} = \sqrt{\frac{S_{0V} - S_{1V}}{S_{0H} + S_{1H}}} \tag{11b}$$

where S_{0V} and S_{1V} (S_{0H} and S_{1H}) are the first and the second components of the emergent Stokes vector when the incident Stokes vector is vertical (horizontal).

In the same way, the phase shift Δ can be deduced by applying either a linear polarization at 45° or a right circular polarization:

$$\Delta = \text{ArcTan}\left[\frac{S_{3_{45}}}{S_{2_{45}}}\right] = \text{ArcTan}\left[\frac{S_{3R}}{S_{2R}}\right] \tag{12}$$

S_{245} and S_{345} (S_{2R} and S_{3R}) are the third and the fourth components of the emergent Stokes vector when the incident Stokes vector is linear oriented at 45° (right circular).

In terms of the elements of the Mueller matrix M_{ref} the normalized reflection coefficient is completely defined by:

$$\rho_0 = \frac{\rho_P}{\rho_S} = \sqrt{\frac{m_{00} + m_{11} - m_{01} - m_{10}}{m_{00} + m_{01} + m_{10} + m_{11}}} \tag{13}$$

$$\Delta = \text{ArcTan}\left[\frac{1}{2}\left(\frac{m_{32}}{m_{22}} - \frac{m_{23}}{m_{33}}\right)\right] \tag{14}$$

3.5. Estimation of the normalized reflection coefficient from the polar decomposition

The normalized reflection coefficient can also be estimated directly from the parameters coming from the polar decomposition of the Mueller matrix (retardance and diattenuation). The application of the polar decomposition onto a Mueller matrix returns the full polarimetric

characterization of the medium or the element described by the matrix. As shown by the equation (5), The polar decomposition gives retardance diattenuation, and depolarization properties.

Retardance represents the difference in phase accumulation between two polarization states. The retardance has three degrees of freedom which can be expressed as the horizontal-vertical retardance, the 45°-135° linear retardance and the right-left circular retardance. The diattenuation, which refers to the difference in attenuation between two orthogonal states, has also the same three degrees of freedom. The phase shift between the S and P components corresponds to the linear retardance R_L. The change in the amplitude ratio between these two components S and P is deduced from the linear diattenuation D_L.

$$R_L = \sqrt{D^2_H + D^2_{45}} \tag{15}$$

$$D_L = \sqrt{D^2_H + D^2_{45}} \tag{16}$$

$$\rho = (1 - D_L).\mathrm{Exp}[i.R_L] \tag{17}$$

3.6. Determination of the refractive index from the solution of the fundamental equation of ellipsometry

The solution of the fundamental equation of ellipsometry is obtained by expressing the Fresnel's coefficients in reflection (equation 1) from the refractive index of the medium and the angle of incidence θ_i. The final expression for r_p and r_s is obtained by using the Snell's law of refraction.

$$\mathrm{Sin}\theta_r = \frac{1}{n}\sin\theta_i \tag{18}$$

Equation (3) can then be rewritten as:

$$\rho = \frac{n^2\cos\theta_i - \sqrt{n^2 - \sin^2\theta_i}}{n^2\cos\theta_i + \sqrt{n^2 - \sin^2\theta_i}} \cdot \frac{\cos\theta_i + \sqrt{n^2 - \sin^2\theta_i}}{\cos\theta_i - \sqrt{n^2 - \sin^2\theta_i}} \tag{19}$$

The resolution of the equation (19) leads finally to the solution of the fundamental equation of ellipsometry which expresses the refractive index n versus the normalized reflection coefficient and the angle of incidence:

$$n = \sin\theta_i \left[1 + \left(\frac{1-\rho}{1+\rho} \right)^2 . \tan^2\theta_i \right]^{1/2} \tag{20}$$

3.7. Precision on the estimation of the refractive index

The determination of the refractive index is straightforward if we applied the polar decomposition. However, this second method does not permit us to estimate the precision onto the refractive index from the errors on the elements of the Mueller matrix. The first method is preferable because it gives the expression of the normalized reflection coefficient from the m_{ij} coefficients. The precision on the refractive index can then be obtained from the error function defined by:

$$\varepsilon_n = \sqrt{\left(\frac{\partial n}{\partial \theta_i} \right)^2 \Delta\theta_i + \left(\frac{\partial n}{\partial m_{00}} \right)^2 \Delta m_{00} + \left(\frac{\partial n}{\partial m_{01}} \right)^2 \Delta m_{01} + \ldots + \left(\frac{\partial n}{\partial m_{33}} \right)^2 \Delta m_{33}} \tag{21}$$

where each derivative is deduced from the equation (20) by expressing the normalized reflection coefficient in terms of the m_{ij} coefficients. The terms Δm_{ij} are deduced from the data resulting from a calibration of the Mueller matrix imaging polarimeter.

4. Results

4.1. Estimation of the refractive index for the spherical targets

The refractive index of each spherical target was estimated by using the first method previously described. The area from which the average Mueller matrix has been determined was not large enough to provide a good estimation of the refractive index. Furthermore, the bistatic angle for these measurement was about 10 degrees, which gives an angle of incidence of about 5 degrees. In these conditions the reflection coefficients r_p and r_s have almost the same magnitude. As the normalized reflection coefficient is deduced from the ratio of the reflection coefficients, a small variation on the magnitude of r_p and r_s can produce a large error on the final result. The refractive index obtained for each target is given on table 1. They are given only as example and must not be considered as good. Most of the parameters used for their determination (mainly the angle of incidence) were not precise enough to get a good estimation.

	Estimation of the refractive index from M_{Ref}
Stainless steel sphere	$\rho_0 = 0.9683$ $\Delta = -0.0098$ rad. **$\rho = -0.9682 + 0.0094\ I$** **$n = 0.531\ (1 - 0.294\ I)$**
Ping-pong ball	$\rho_0 = 0.9955$ $\Delta = -0.0131$ rad. **$\rho = -0.9955 + 0.013\ I$** **$n = 0.430\ (1 - 2.936\ I)$**
Plastic sphere	$\rho_0 = 1.0038$ $\Delta = -0.0004$ rad. **$\rho = -1.0038 + 0.0004\ I$** **$n = 4.814\ (1 - 0.104\ I)$**
Wooden sphere	$\rho_0 = 1.0335$ $\Delta = -0.0027$ rad. **$\rho = -1.0335 + 0.0028\ I$** **$n = 0.564\ (1 - 0.079\ I)$**

Table 1: Refractive index of each spherical target deduced from the Mueller matrix image.

4.2. Estimation of the refractive index of metal and glass plates

As shown on the precedent section, the estimation of the refractive index from the polarization signatures of spherical targets is not obvious when the angle of incidence is very small. We have extended our method in the case of object with plane surfaces in order to validate our estimation method. Four new objects were measured at an angle of incidence of 45 degrees corresponding to:

- an aluminum plate
- a steel plate
- microscope slide (borosilicate glass)
- a plexiglass plate

The refractive index was measured from the average Mueller matrix deduced from a large area (see Table 2) and for each individual pixel in order to get an estimation of the variation of the refractive index over the surface analyzed. The average refractive index for each material is given on Table 2.

	Average refractive index	
Aluminum plate	**$n = 0.388\ (1 - 12.677\ I)$** **$\varepsilon_n = \pm(0.013+0.159\ I)$**	**Nb. Of pixels averaged: 500**
steel plate	**$n = 1.308\ (1 - 4.058\ I)$** **$\varepsilon_n = \pm(0.046+0.170\ I)$**	**Nb. Of pixels averaged: 400**
plexiglass	**$n = 1.536\ (1 - 0.010\ I)$** **$\varepsilon_n = \pm(0.043+0.0008\ I)$**	**Nb. Of pixels averaged: 400**
Microscope slide	**$n = 1.697\ (1 - 0.006\ I)$** **$\varepsilon_n = \pm(0.049+0.0004\ I)$**	**Nb. Of pixels averaged: 1200**

Table 2: Average refractive index.

Metal plates (aluminum and steel) are both conducting materials and thus present a high extinction coefficient. The value of the refractive index of aluminum for deposited film given in the literature is n = 1.02, k = 7.26 for λ = 600 nm. The large difference between our estimation and the value found could be explained first by the bad optical quality of our sample and by the relatively large variations of the optical constants with temperature as mentioned in the reference used [4]. No reference has been found for the second sample (steel), furthermore steel is not a pure metal but a compound and such a material can have large variation of its optical constants according to its composition. We give here for comparison the refractive index for iron at 590 nm: n = 2.80, k = 3.34.

The last two samples are transparent materials which imply, as found by the measurement, a null extinction coefficient. The value of the refractive index of the plexiglass given by a manufacturer (PLASTEC, Inc.) is n = 1.488 at 656 nm. The experimental value obtained (n = 1.536) is greater than we should expected but remains in agreement with the value given by the manufacturer. The microscope slide made of a borosilicate glass gives a refractive index of 1.697. The value of the refractive indices found in the literature [5] for borosilicate glasses (Bk7, BalK1, SK4, SSK4) are comprised between 1.51 (BK7) and 1.61 (SSK4) which is, in any case, inferior to the estimation of the refractive index of the microscope slide.

The estimated refractive indices than can be used to approximate the reflection coefficients r_p and r_s using equations (1a) and (1b). Table 3 gives r_p and r_s for the angle of incidence of 45°. Shown on Figure 8 are the magnitude of the reflection coefficients r_p and r_s deduced from the estimated refractive index of the aluminum plate. The magnitude of the reflection coefficients of the other samples are given in Appendix D.

	Reflection coefficients r_p and r_s
Aluminum plate	**r_p = 0.81-0.51 I** **r_s = -0.94+0.27 I**
steel plate	**r_p = 0.78-0.42 I** **r_s = -0.91+0.23 I**
plexiglass	**r_p = 0.100-0.003 I** **r_s = -0.317+0.006 I**
Microscope slide	**r_p = 0.138+0.002 I** **r_s = -0.37-0.003 I**

Table 3: Reflection coefficients r_p and r_s for $\theta_i = 45°$.

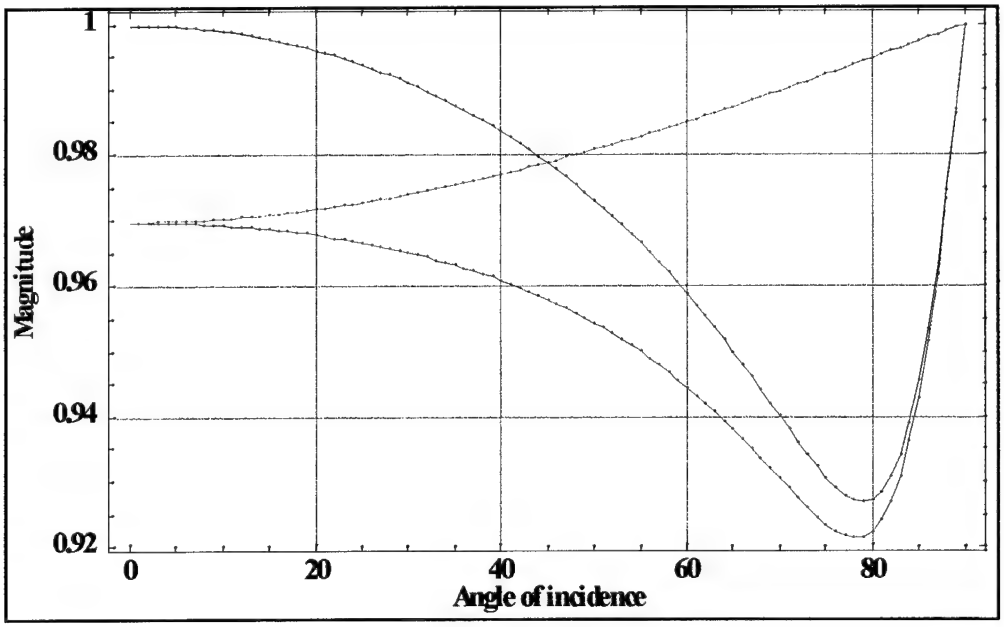

Figure 8: Reflection coefficients r_p (red) and r_s (green) of aluminum versus the angle of incidence (normalized reflection coefficient in blue).

4.3. Dispersion of the refractive index

The dispersion of the refractive index is determined by estimating n for each individual pixel of the image used to calculate the average Mueller matrix. As shown on Figure 9, The dispersion of the normalized reflection coefficient is relatively small but it introduces a huge dispersion on the refractive index. From this graph, it is obvious that an estimation of the refractive index can be difficulty obtained when the normalized reflection coefficient is calculated from only a few pixels. This also explains the difficulty we had to extract a correct value of the refractive index from the polarization signatures of the spherical targets.

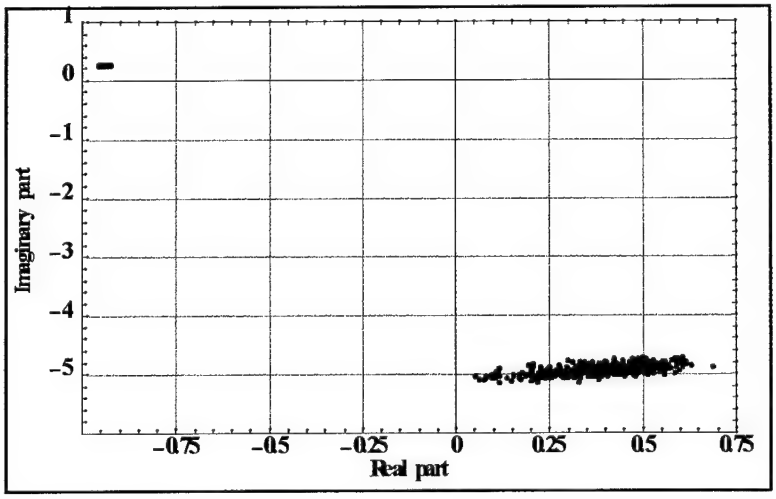

Figure 9: Dispersion of the normalized reflection coefficient (Blue) and the refractive index (red) for aluminum.

The dispersions obtained for each refractive index are given on Appendix C. The relative variations of the real and imaginary parts are defined as:

$$\Delta X = \frac{X_{Max} - X_{Min}}{X_{Mean}} \tag{22}$$

where X_{Max} and X_{Min} are the maximum and minimum values of the real and the imaginary parts of the refractive index. X_{mean} is the mean value of the real or imaginary part of n determined from the summation of the refractive index of each pixel.

5. Conclusion

During this second phase two aspects of the polarization have been studied. The first part was an extension of the first phase and concerned the study of the behavior of the polarization signatures according to the position either of the detection system or the target. As shown on this report, orientation and shape of the target can be estimated whatever its position. But such results must be examined on other types of targets (different in shape, metal, roughness, ...) in order to validate the method and estimate the ability of the technique. However, these first results show the strong potential of the PDAI technique for estimating orientation and shape of objects using polarimetry.

The second phase of this research program has investigated a calculation method to estimate the refractive index from the polarization signature of the targets. Refractive index is directly deduced from the totally polarized part of the normalized Mueller matrix (retardance and diattenuation). As shown on appendix D, the calculation method gives some good estimations of the refractive index but the variations of the results yet remain important. The origin of this variation is due to the fact that the refractive index is determined from the normalized reflection coefficient. As the normalized reflection coefficient represents the ratio of the s and p reflection coefficients, a variation on one of this coefficient can then induce a large variation on the final result. However, the average refractive indices deduced from this method are in agreement with those found in the literature.

6. References

1. S.-Y. Lu and R.A. Chipman, "Interpretation of Mueller matrices based on polar decomposition, *J. Opt. Soc. Am. A* **13**(5) (1996).

2. R.M.A. Azzamand N.M. Bashara, *Ellipsometry and Polarized Light*, North-Holland, Amsterdam, (1977).

3. E. Collett, Polarized Light: Fundamentals and Applications, Marcel Dekker, Inc., New-York (1993)

4.R.A. Paquin, "Properties of Metals," in the *Handbook of Optics*, Chap. 35 (McGraw-Hill, New York, 1994).

5. W.J. Tropf, M.E. Thomas, T.J. Harris, "Properties of Crystals and Glasses," in the *Handbook of Optics*, Chap. 33 (McGraw-Hill, New York, 1994).

Appendix A

The Mueller Matrix Imaging Polarimeter

The Mueller Matrix Imaging Polarimeter

1. Principle

The Mueller Matrix Imaging Polarimeter (MMIP) was constructed at UAH under an AFOSR grant issued in 1989 by program manager Lee Giles. The Mueller Matrix Imaging Polarimeter took three years to assemble and calibrate before accurate Mueller matrix images were being routinely measured, an indication of the complexity of the technique. The instrument formed the basis for Larry Pezzaniti's dissertation, which contains a wealth of information on the technique. The Mueller matrix imaging polarimeter has become the most successful instrument in the Polarization Laboratory and has been involved in over 30 papers.

The Mueller Matrix Imaging Polarimeter is an accurate instrument for measuring polarization properties over a field of view in visible and near-infrared light. The MMIP can measure the polarization and polarization scrambling properties of optical elements at a high resolution [1]. This instrument can be configured for measurements in transmission, reflection, retro reflection, and variable-angle scattering. The MMIP has been used for characterization of polarization elements, beam splitter cubes[2], scattering surfaces [3], liquid crystal modulators[4], electro-optic PLZT modulators [5], GaAs waveguide devices[6], and entire optical systems.

For Polarization Diversity Active Imaging the sample becomes a target, and the polarization generator and polarization analyzer are configured for bistatic scattering measurements. All of the polarization altering properties of the sample, the diattenuation, retardance, depolarization, and polarizance, may be computed from the Mueller matrix. Diattenuation refers to the difference in attenuation between two orthogonal polarization states (sometimes referred to as the polarizing efficiency), retardance is the difference in phase accumulation between two polarization states, depolarization is the coupling of polarized light into unpolarized light, and polarizance is the coupling of unpolarized light into polarized light.

Shown in figure 1 in its current configuration for scattering measurements, the polarimeter may be divided into three sections: a polarization state generator, a sample compartment, and a polarization state analyzer. The polarization state generator includes a spatially filtered laser whose coherence has been scrambled by a spinning groung glass plate in order to remove speckle effects. The instrument presently operates with a 633nm He-Ne 5mw laser, a 1064 nm YAG laser (200 mW), a 543 nm 15 mW HeNe, and a 850nm 25mw diode laser, although configuring the instrument with a new source is straightforward.

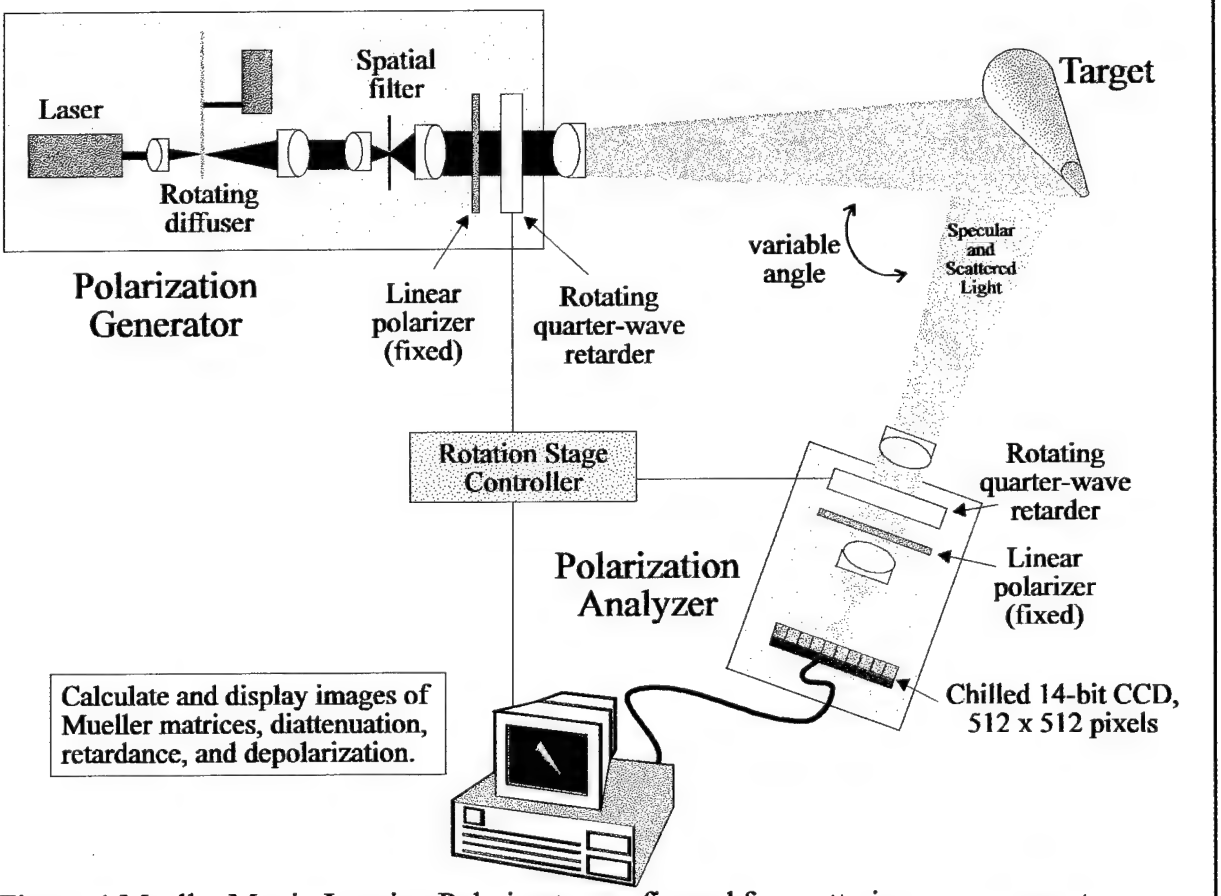

Figure 1 Mueller Matrix Imaging Polarimeter configured for scattering measurements

The MMIP is a dual-rotating retarder polarimeter which illuminates a sample with known polarized states and then analyzes the exiting polarized state over a spatially-resolved image of the sample. Highly calibrated polarization optics are used in the measuring instrument, and an extensive

calibration procedure is followed to ensure the accuracy of the measurements . Figure 1 shows the configuration of the MMIP in transmission. It consists of a sample compartment placed between a polarization state generator and a polarization state analyzer, each composed of a stationary linear polarizer and a rotating quarter-wave linear retarder. Images at 60 different orientations of the rotating retarders are used to measure a Mueller matrix image. The Mueller matrix image is measured by capturing the sixty different intensity images of the target. The only change between the images is the orientations of the retarders in the polarization generator and analyzer which induce an intensity change on the images. The 60 images are processed into a 16-elements Mueller matrix image [7] using a Mathematica package of data reduction and analysis algorithm developed by our research group . Each Mueller matrix M is obtained according to the optimal (least-squares) polarimetric data reduction equation using the pseudoinverse matrix W_P^{-1} of W where W is the polarimetric data reduction matrix of the polarimeter:

$$\mathbf{M} = (\mathbf{W}^{T}\mathbf{W})^{-1}\mathbf{W}^{T}\mathbf{I} = \mathbf{W}_{P}^{-1}\mathbf{I} \tag{1}$$

W is a matrix of dimension 16×60 describing the full sequence of measurements, and I is a measurement vector of dimension 60 representing a set of sixty intensities.

The 4-by-4 Mueller matrix, **M**, relates an incident polarized state described by Stokes vector $\vec{S}$ to the exiting (reflected, transmitted, scattered) state with Stokes vector $\vec{S}'$:

$$\vec{S}' = \begin{bmatrix} S_0' \\ S_1' \\ S_2' \\ S_3' \end{bmatrix} = \mathbf{M}\vec{S} = \begin{bmatrix} m_{00} & m_{01} & m_{02} & m_{03} \\ m_{10} & m_{11} & m_{12} & m_{13} \\ m_{20} & m_{21} & m_{22} & m_{23} \\ m_{30} & m_{31} & m_{32} & m_{33} \end{bmatrix} \begin{bmatrix} S_0 \\ S_1 \\ S_2 \\ S_3 \end{bmatrix} \tag{2}$$

The Mueller matrix can be written as the multiplication of a pure depolarizing matrix, **D**, a pure retarder matrix, **R**, and a pure diattenuating (polarizing) matrix, **P**:

$$\mathbf{M} = \mathbf{D}\cdot\mathbf{R}\cdot\mathbf{P} \tag{3}$$

These 4-by-4 matrix images can then be decomposed into images of the depolarization, retardance, and diattenuation [8]. These maps give a spatially-resolved description of the polarization performance of the sample.

The illuminating source for these measurements was a 5mW HeNe laser operating at a wavelength of 632.8nm. The target (cone) is illuminated with collimated light; the specularly reflected and scattered light passes through the polarization analyzer and is detected on the CCD array.

2. References

1. J.L. Pezzaniti and R.A. Chipman, "Mueller matrix imaging polarimetry," *Opt. Eng.* **34**(6), 1558-1568 (1995).

2. J.L. Pezzaniti and R.A. Chipman, "Angular dependence of polarizing beam splitter cubes," *Appl. Opt.* **33**(10), 1916-1929 (1994).

3. J.L. Pezzaniti and R.A. Chipman, "Mueller matrix scatter polarimetry of a diamond-turned mirror," *Opt. Eng.* **34**(6), 1593-1598 (1995).

4. J.L. Pezzaniti, S.C. McClain, R.A. Chipman, S.-Y. Lu, "Depolarization in a liquid crystal TV's," *Opt. Lett.* **18**(23), 2071-2073 (1993).

5. E.A. Sornsin and R.A. Chipman, "Mueller matrix polarimetry of PLZT electro-optic modulators," *Proc. SPIE* **2873**, (1996).

6. M.H. Smith, E.A. Sornsin, R.A. Chipman, T.J. Tayag, "Polarization characterization of self-imaging GaAs/AlGaAs waveguide beamsplitters using Mueller matrix imaging polarimetry," submitted to SPIE Photonics West `97 (Optoelectronics, 1997).

7. R.A. Chipman, "Polarimetry," in the *Handbook of Optics*, Chap. 22 (McGraw-Hill, New York, 1994).

8. S.-Y. Lu and R.A. Chipman, "Interpretation of Mueller matrices based on polar decomposition, *J. Opt. Soc. Am. A* **13**(5) (1996).

Appendix B

Retardance and diattenuation
ligne graph images of the brass cone.

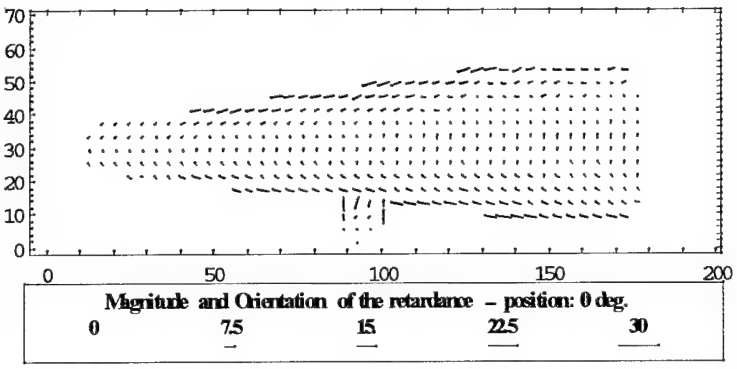
70
60
50
40
30
20
10
0
0
50
100
150
200
Magnitude and Orientation of the retardance – position: 0 deg.
0
7.5
15
22.5
30

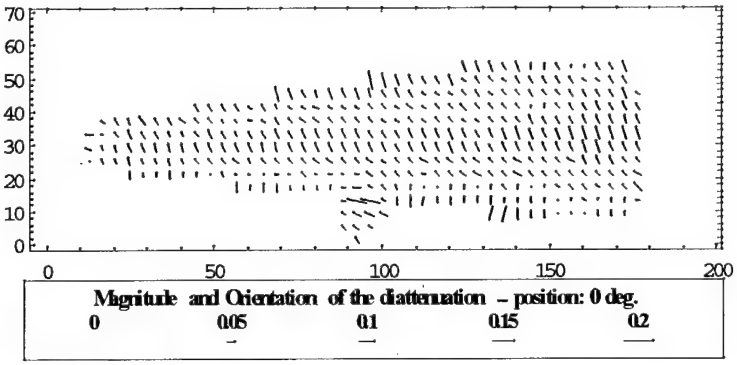
70
60
50
40
30
20
10
0
0
50
100
150
200
Magnitude and Orientation of the diattenuation – position: 0 deg.
0
0.05
0.1
0.15
0.2

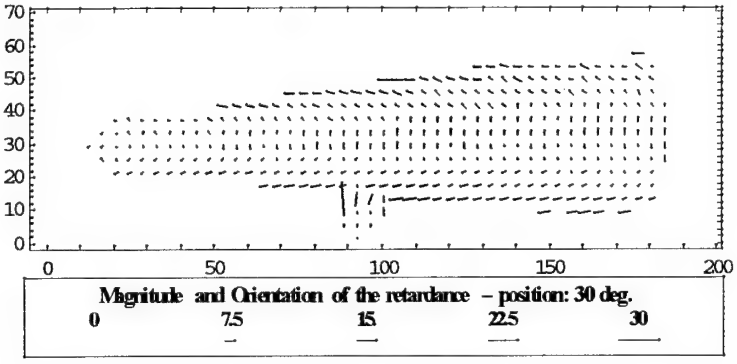
70
60
50
40
30
20
10
0
0
50
100
150
200
Magnitude and Orientation of the retardance – position: 30 deg.
0
7.5
15
22.5
30

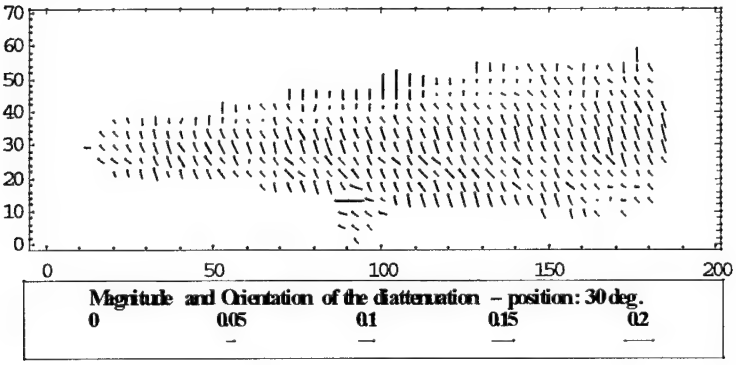
70
60
50
40
30
20
10
0
0
50
100
150
200
Magnitude and Orientation of the diattenuation – position: 30 deg.
0
0.05
0.1
0.15
0.2

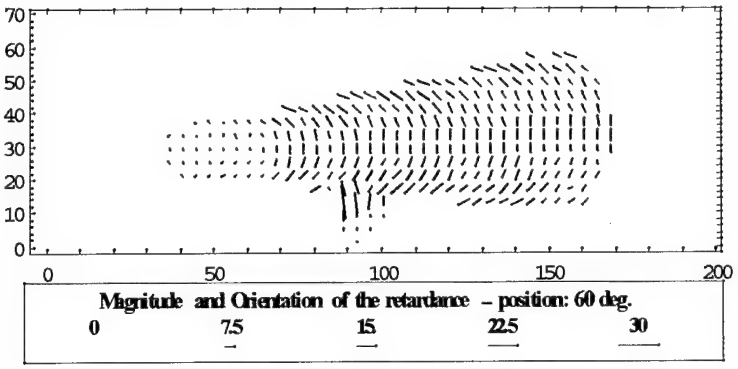
70
60
50
40
30
20
10
0
0
50
100
150
200
Magnitude and Orientation of the retardance – position: 60 deg.
0
7.5
15
22.5
30

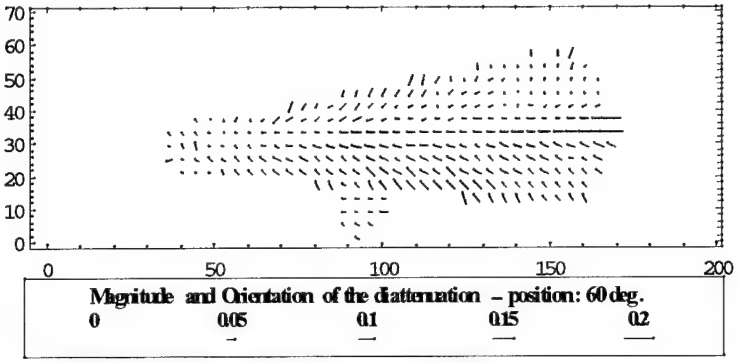
70
60
50
40
30
20
10
0
0
50
100
150
200
Magnitude and Orientation of the diattenuation – position: 60 deg.
0
0.05
0.1
0.15
0.2

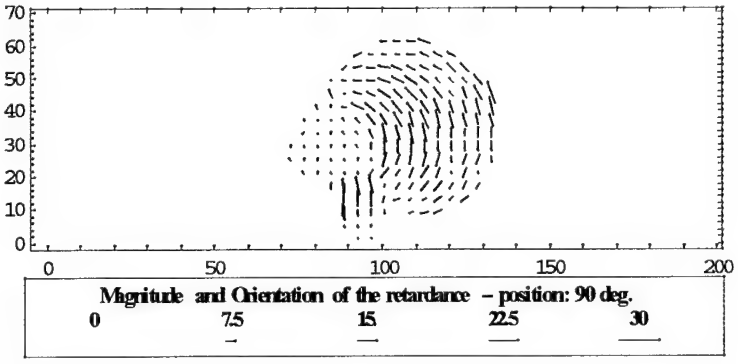
70
60
50
40
30
20
10
0
0
50
100
150
200
Magnitude and Orientation of the retardance – position: 90 deg.
0
7.5
15
22.5
30

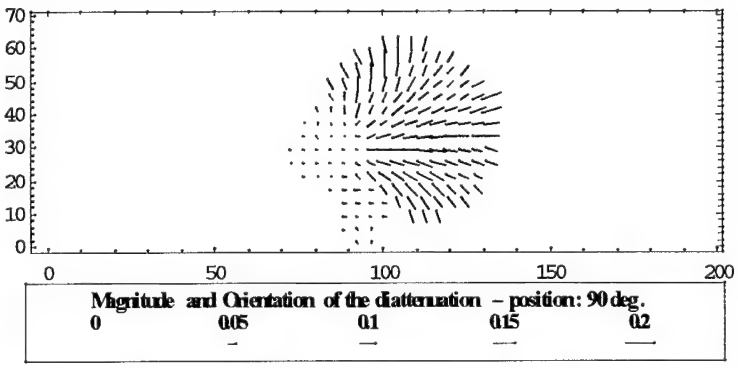
70
60
50
40
30
20
10
0
0
50
100
150
200
Magnitude and Orientation of the diattenuation – position: 90 deg.
0
0.05
0.1
0.15
0.2

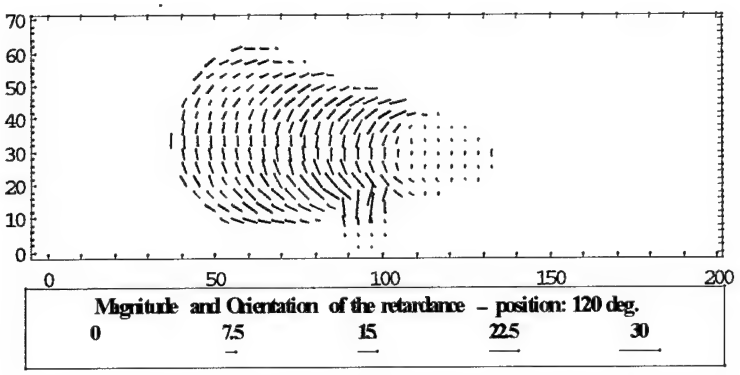
70
60
50
40
30
20
10
0
0
50
100
150
200
Magnitude and Orientation of the retardance – position: 120 deg.
0
7.5
15
22.5
30

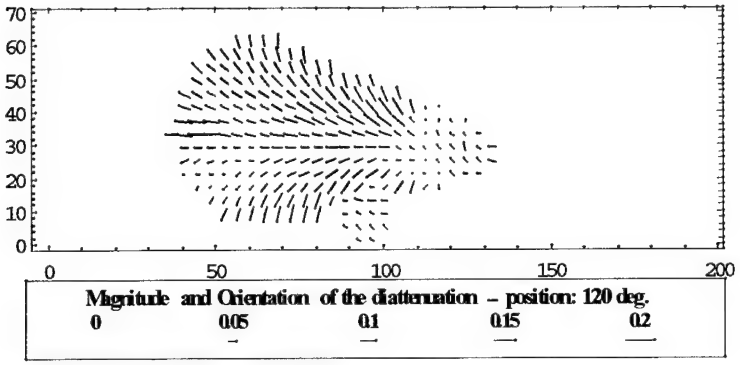
70
60
50
40
30
20
10
0
0
50
100
150
200
Magnitude and Orientation of the diattenuation – position: 120 deg.
0
0.05
0.1
0.15
0.2

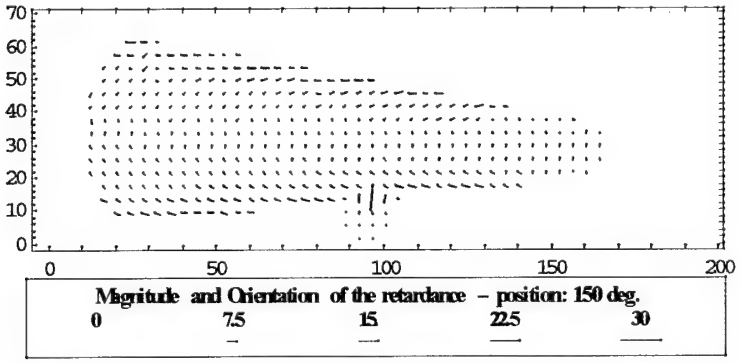
70
60
50
40
30
20
10
0
0
50
100
150
200
Magnitude and Orientation of the retardance – position: 150 deg.
0
7.5
15
22.5
30

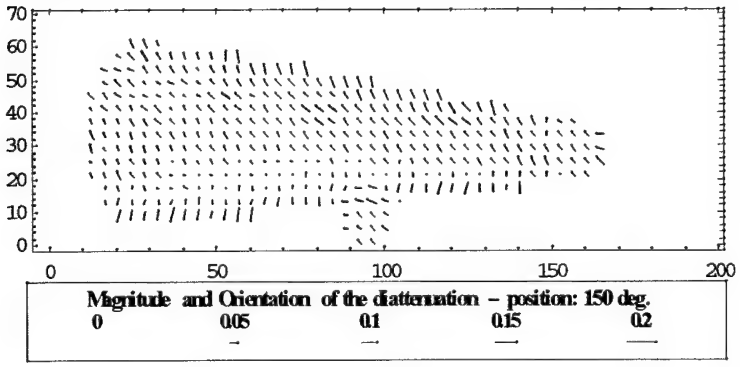
70
60
50
40
30
20
10
0
0
50
100
150
200
Magnitude and Orientation of the diattenuation – position: 150 deg.
0
0.05
0.1
0.15
0.2

Appendix C

Polarization signatures of the brass cone
for different positions of the polarization analyzer.

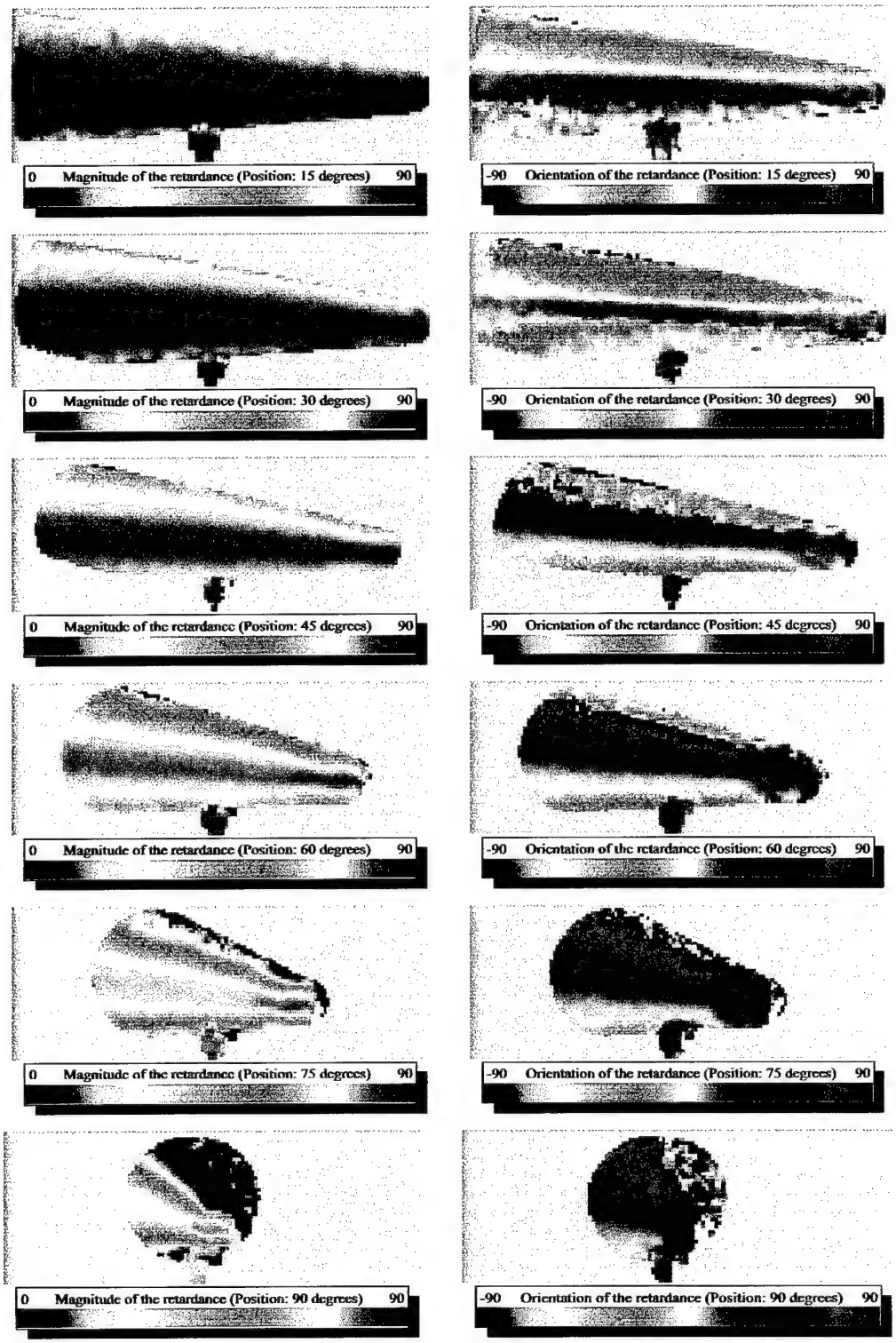

C1: Magnitude and orientation images of the retardance for different positions of the polarization analyzer.

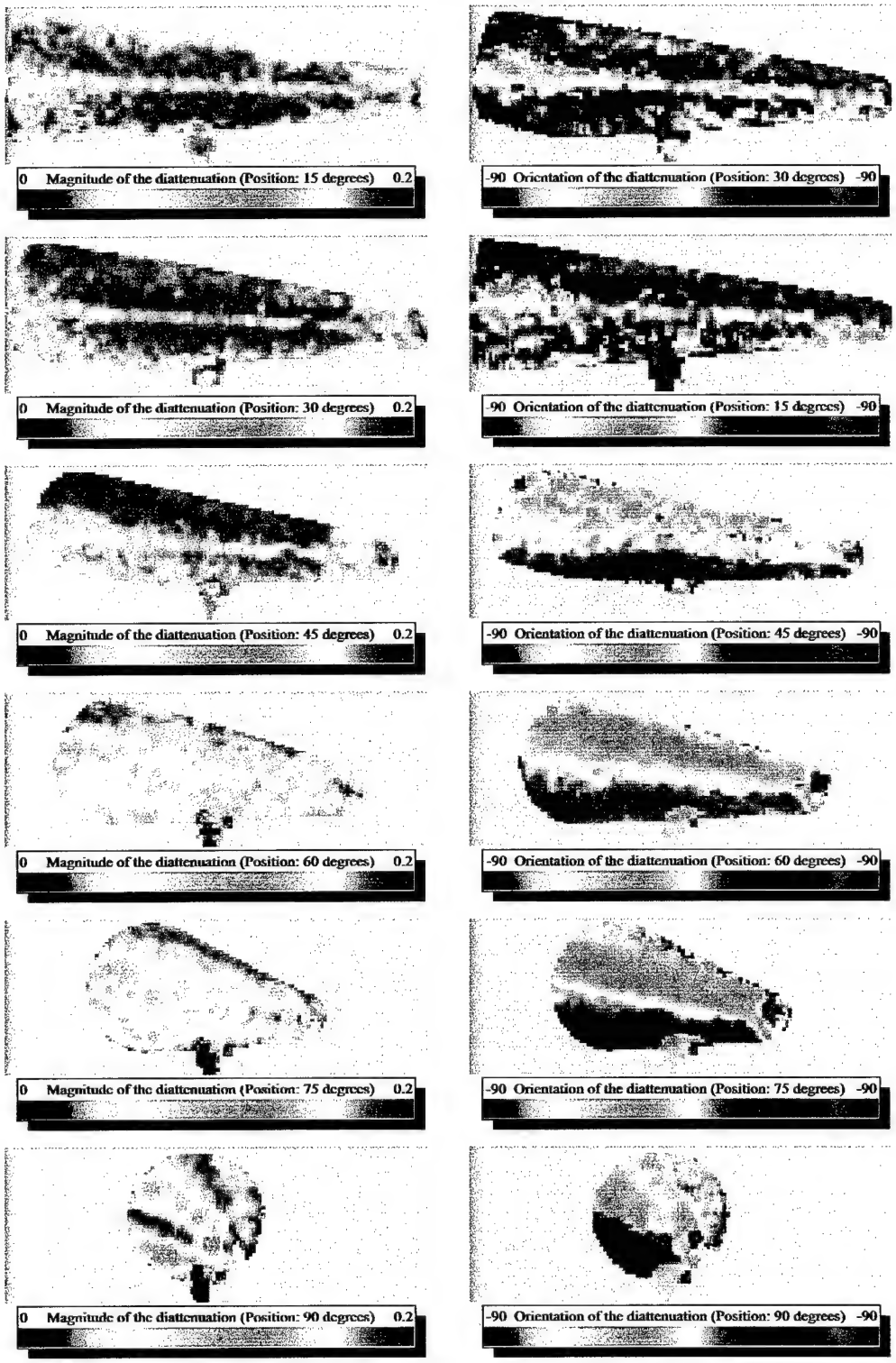

C2: Magnitude and orientation images of the diattenuation for different positions of the polarization analyzer.

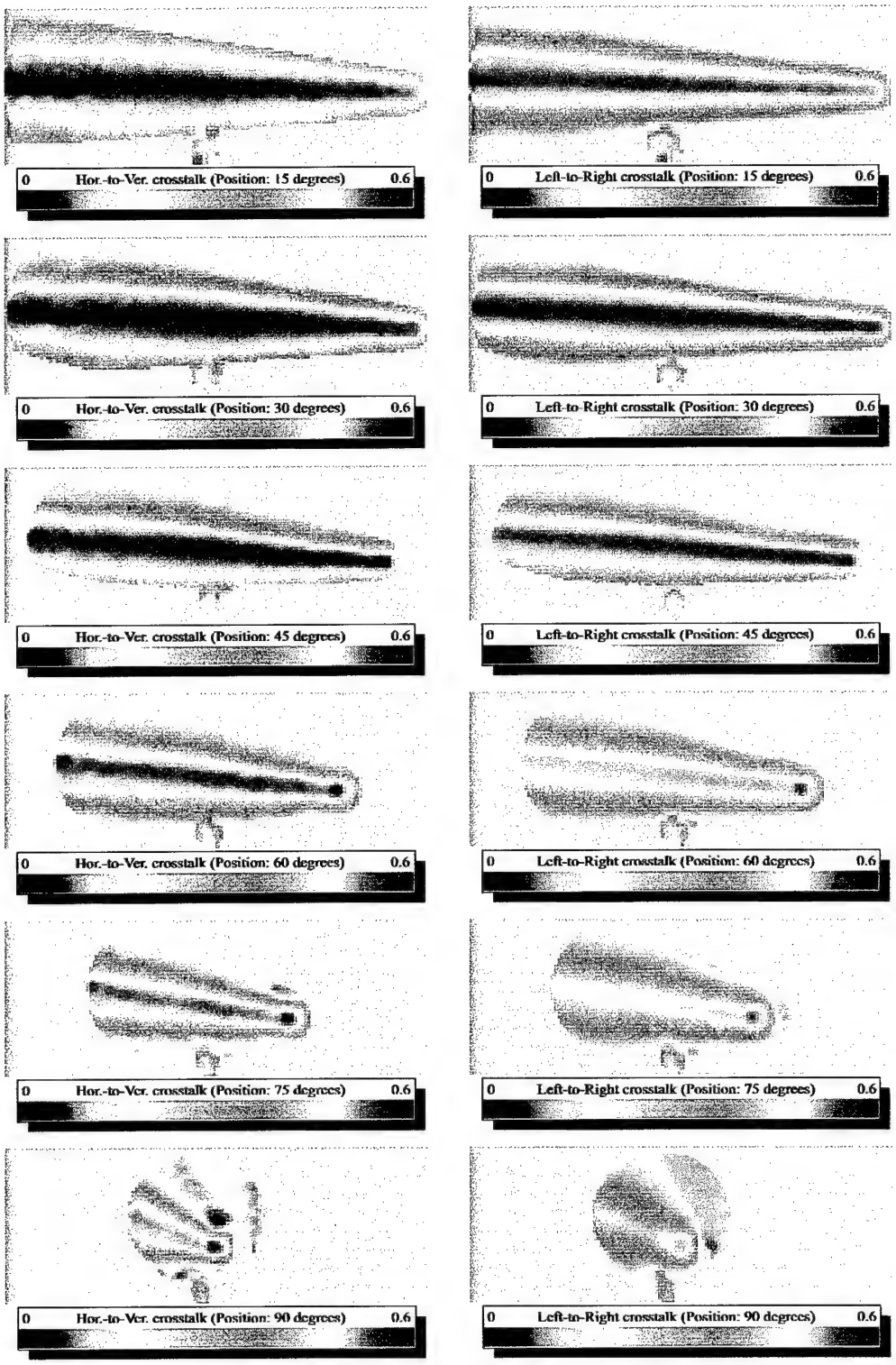

C3: Horizontal-to-vertical and left-to right crosstalk images for different position of the polarization analyzer.

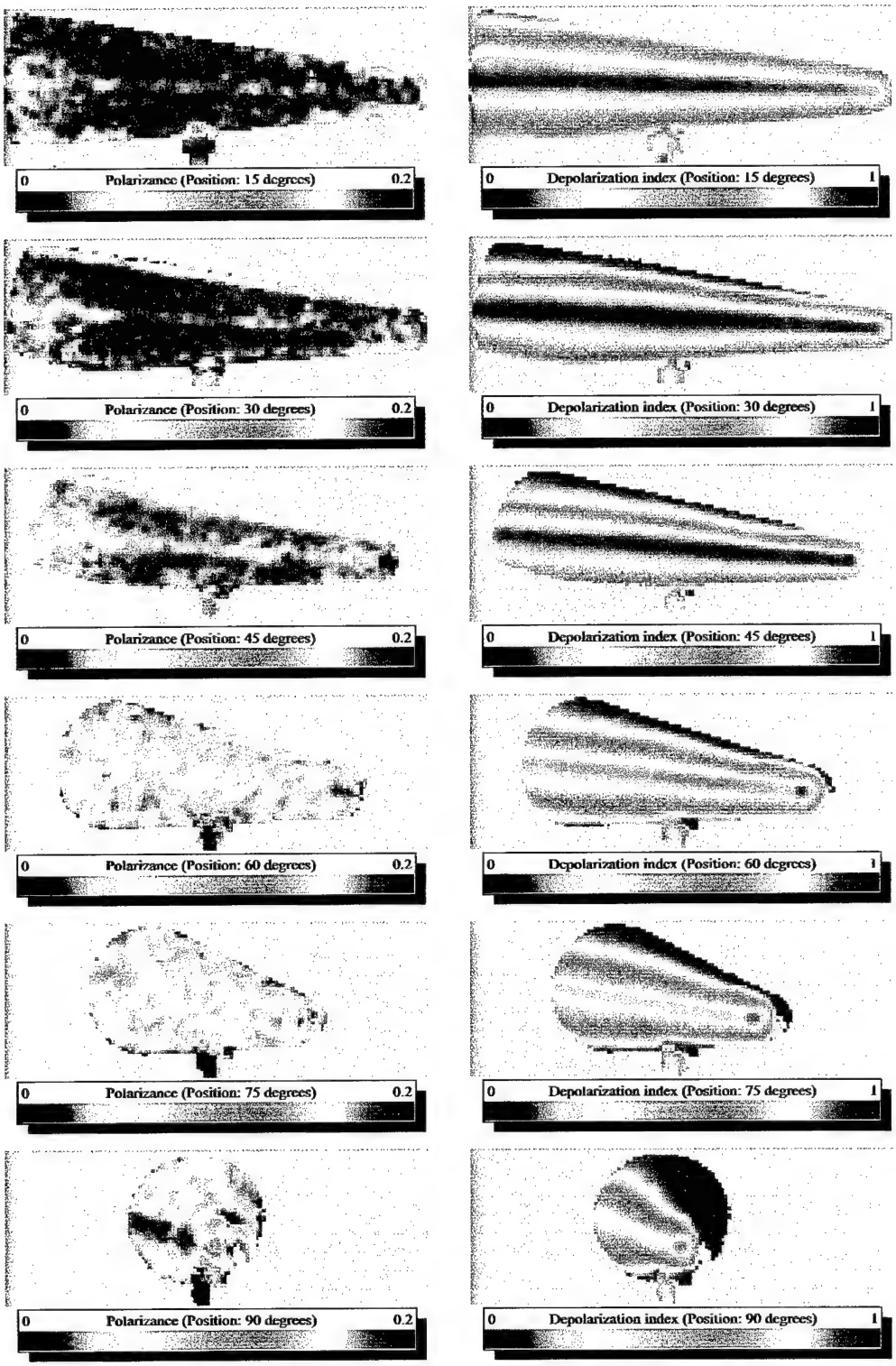

C4: Polarizance and depolarization index images for different positions of the polarization analyzer.

Appendix D

Dispersion of the refractive index

D1. Aluminum plate

Average Mueller matrix: $M = \begin{bmatrix} 1 & -0.0214 & 0.0005 & -0.0010 \\ -0.0332 & 0.9968 & 0.0034 & 0.0023 \\ -0.0003 & -0.0075 & 0.9515 & 0.2789 \\ -0.0011 & 0.0006 & -0.2713 & 0.9565 \end{bmatrix}$

Normalized reflection coefficient: $\rho = -0.9404 + 0.2712\ I$

Refractive index: 0.3884 - 4.9239 I

Orientation of the first eigen-direction:	-0.150°
Orientation of the second eigen-direction:	-89.912°
Inhomogeneity:	0.004
Magnitude of the normalized reflection coefficient:	0.9788
Phase shift induced by the reflection:	-16.088°

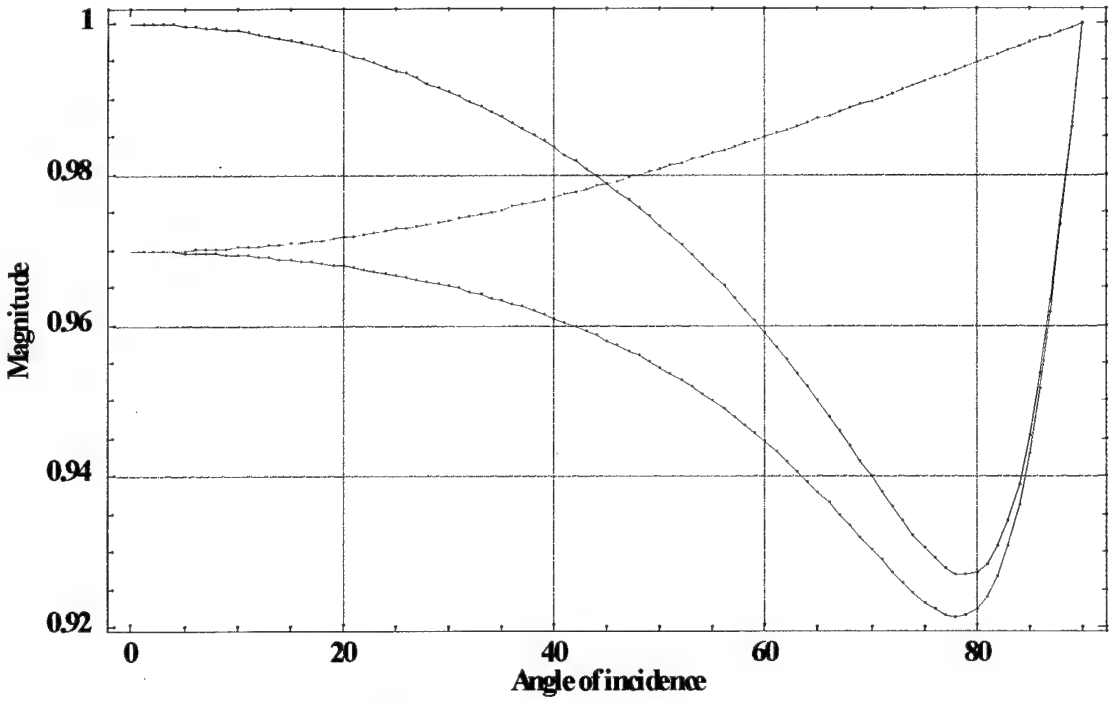

Figure D1: Reflection coefficients r_p (red ligne) and r_s (green ligne) of aluminum versus the angle of incidence (normalized reflection coefficient in blue ligne).

Dispersion of the normalized reflection coefficient:

- mean value of the real part:	-0.9404
- standard deviation of the real part:	0.0068
- mean value of the imaginary part:	0.2712
- standard deviation of the imaginary part:	0.0031

Dispersion of the refractive index:

- mean refractive index:	0.3866 - 4.9224 I
- standard deviation of the refractive index:	0.1011 + 0.0520 I
- relative variation of the real part:	164%
- relative variation of the imaginary part:	8.45%

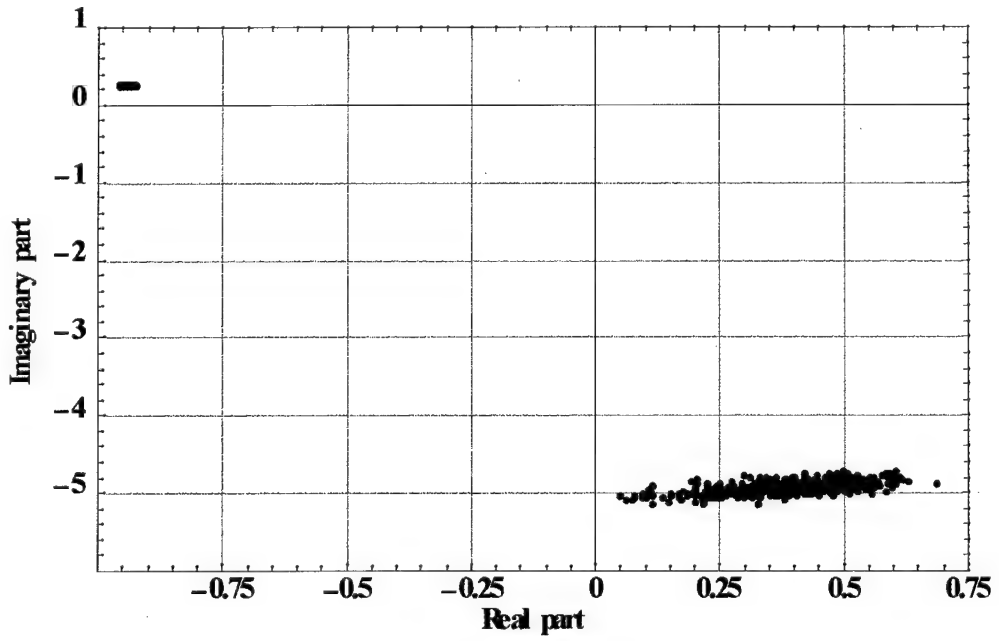

Figure D2: Dispersion of the normalized reflection coefficient (Blue) and the refractive index (red) for aluminum.

D2. Steel plate

Average Mueller matrix: $M = \begin{bmatrix} 1 & -0.0594 & -0.0025 & 0.0061 \\ -0.0839 & 0.9978 & 0.0038 & 0.0071 \\ 0.0044 & 0.0008 & 0.9518 & 0.2473 \\ 0.0073 & -0.0016 & -0.2359 & 0.9540 \end{bmatrix}$

Normalized reflection coefficient: $\rho = -0.9133 + 0.2315\ I$

Refractive index: 1.3088 - 5.3118 I

Orientation of the first eigen-direction:	0.312°
Orientation of the second eigen-direction:	88.716°
Inhomogeneity:	0.027
Magnitude of the normalized reflection coefficient:	0.9422
Phase shift induced by the reflection:	-14.228°

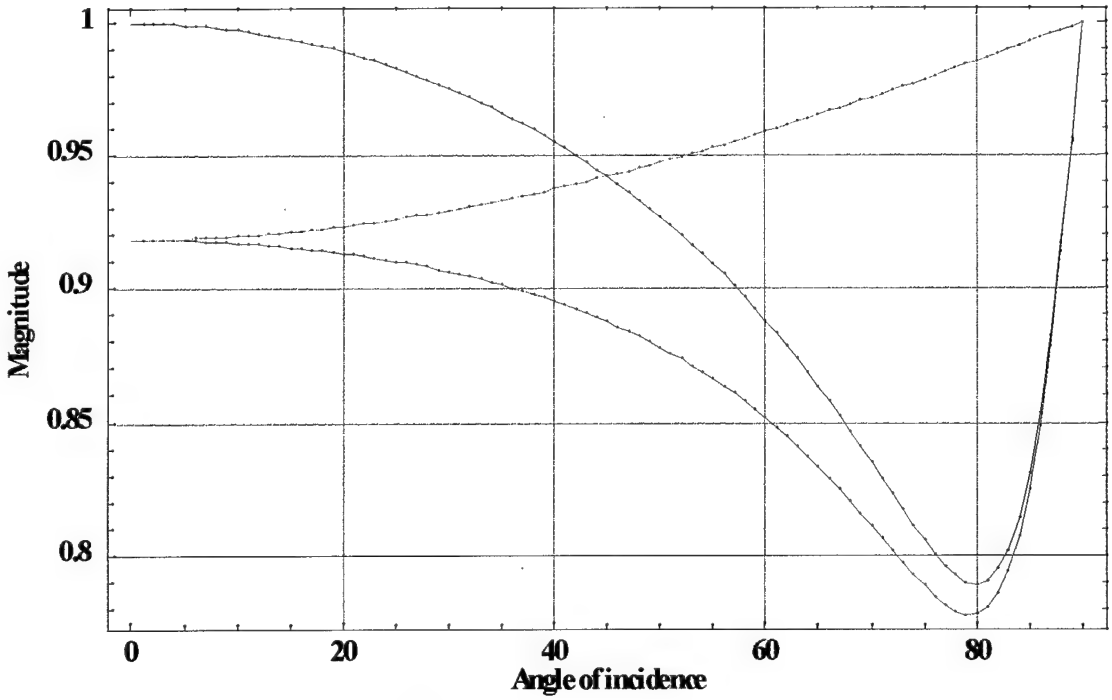

Figure D3: Reflection coefficients r_p (red ligne) and r_s (green ligne) of steel versus the angle of incidence (normalized reflection coefficient in blue ligne).

Dispersion of the normalized reflection coefficient:

- mean value of the real part:	-0.9132
- standard deviation of the real part:	0.0066
- mean value of the imaginary part:	0.2315
- standard deviation of the imaginary part:	0.0069

Dispersion of the refractive index:

- mean refractive index:	1.3066 - 5.3178 I
- standard deviation of the refractive index:	0.0072 + 0.1896 I
- relative variation of the real part:	32%
- relative variation of the imaginary part:	21%

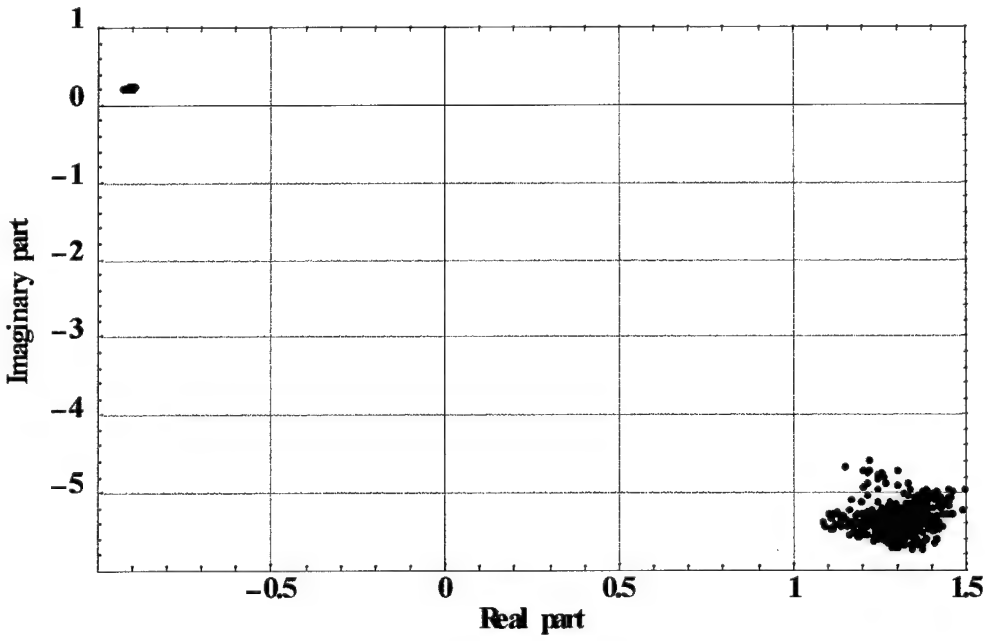

Figure D4: Dispersion of the normalized reflection coefficient (Blue) and the refractive index (red) for steel.

D3. Plexiglass plate

Average Mueller matrix: $M = \begin{bmatrix} 1 & -0.8172 & -0.0037 & 0.0034 \\ -0.8384 & 1.0049 & -0.0783 & 0.0115 \\ -0.0760 & 0.0890 & 0.5328 & 0.0087 \\ -0.0013 & 0.0052 & -0.0131 & 0.5482 \end{bmatrix}$

Normalized reflection coefficient: $\rho = -0.3171 + 0.0061\ I$

Refractive index: 1.5361 - 0.0164 I

Orientation of the first eigen-direction:	0.439°
Orientation of the second eigen-direction:	46.272°
Inhomogeneity:	0.696
Magnitude of the normalized reflection coefficient:	0.317
Phase shift induced by the reflection:	-1.102°

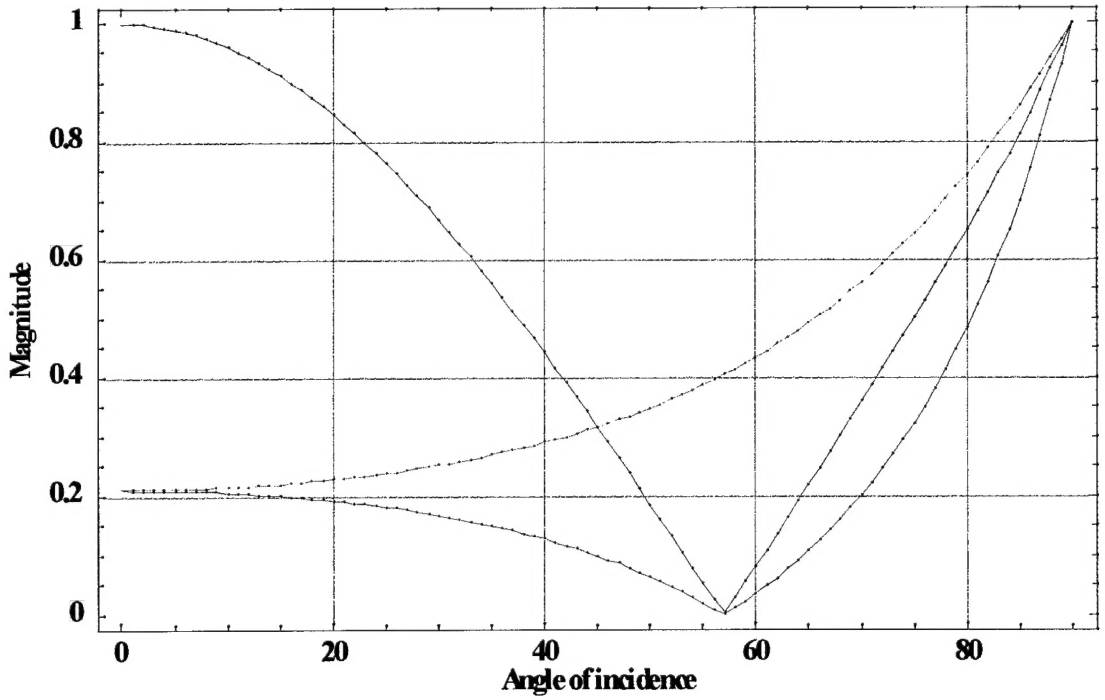

Figure D5: Reflection coefficients r_p (red ligne) and r_s (green ligne) of plexiglass versus the angle of incidence (normalized reflection coefficient in blue ligne).

Dispersion of the normalized reflection coefficient:

- mean value of the real part:	-0.3170
- standard deviation of the real part:	0.0058
- mean value of the imaginary part:	0.0061
- standard deviation of the imaginary part:	0.0021

Dispersion of the refractive index:

- mean refractive index:	1.5361 - 0.0164 I
- standard deviation of the refractive index:	0.0149 + 0.0017 I
- relative variation of the real part:	5.5%
- relative variation of the imaginary part:	221%

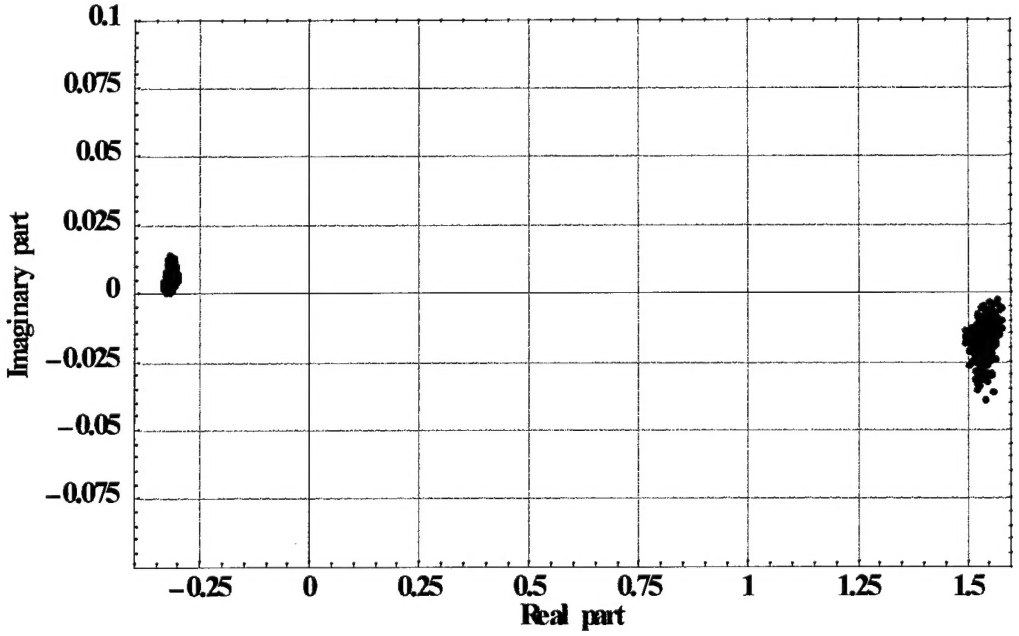

Figure D6: Dispersion of the normalized reflection coefficient (Blue) and the refractive index (red) for plexiglass.

D4. Microscope slide

Average Mueller matrix: $M = \begin{bmatrix} 1 & -0.7587 & -0.0120 & 0.0033 \\ -0.7709 & 0.9473 & -0.0843 & 0.0101 \\ -0.0722 & 0.0905 & 0.5980 & -0.0063 \\ 0.0019 & -0.0013 & -0.0036 & 0.6100 \end{bmatrix}$

Normalized reflection coefficient: $\rho = -0.3715 - 0.0031\ I$

Refractive index: $1.6973 + 0.0101\ I$

Orientation of the first eigen-direction:	-30.012°
Orientation of the second eigen-direction:	3.2908°
Inhomogeneity:	0.8357
Magnitude of the normalized reflection coefficient:	0.3715
Phase shift induced by the reflection:	0.480°

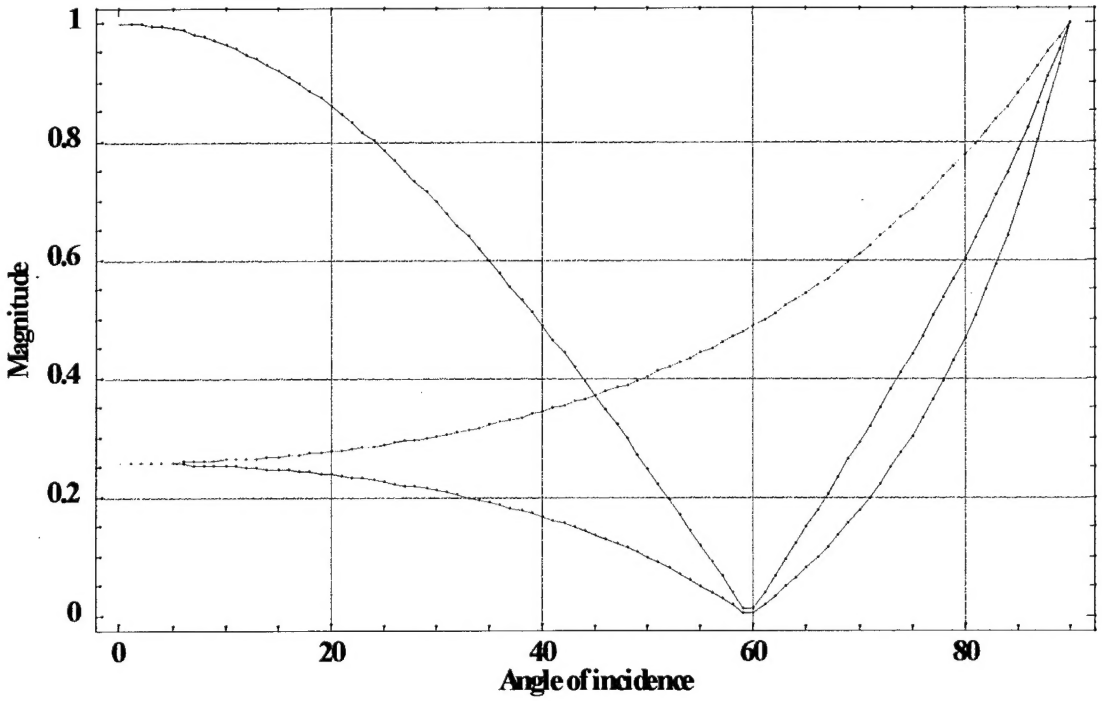

Figure D7: Reflection coefficients r_p (red ligne) and r_s (green ligne) of a microscope slide versus the angle of incidence (normalized reflection coefficient in blue ligne).

Dispersion of the normalized reflection coefficient:

- mean value of the real part:	-0.3468
- standard deviation of the real part:	0.0926
- mean value of the imaginary part:	-0.0030
- standard deviation of the imaginary part:	0.0024

Dispersion of the refractive index:

- mean refractive index:	1.6513 - 0.0098 I
- standard deviation of the refractive index:	0.1748 + 0.0028 I
- relative variation of the real part:	46%
- relative variation of the imaginary part:	565%

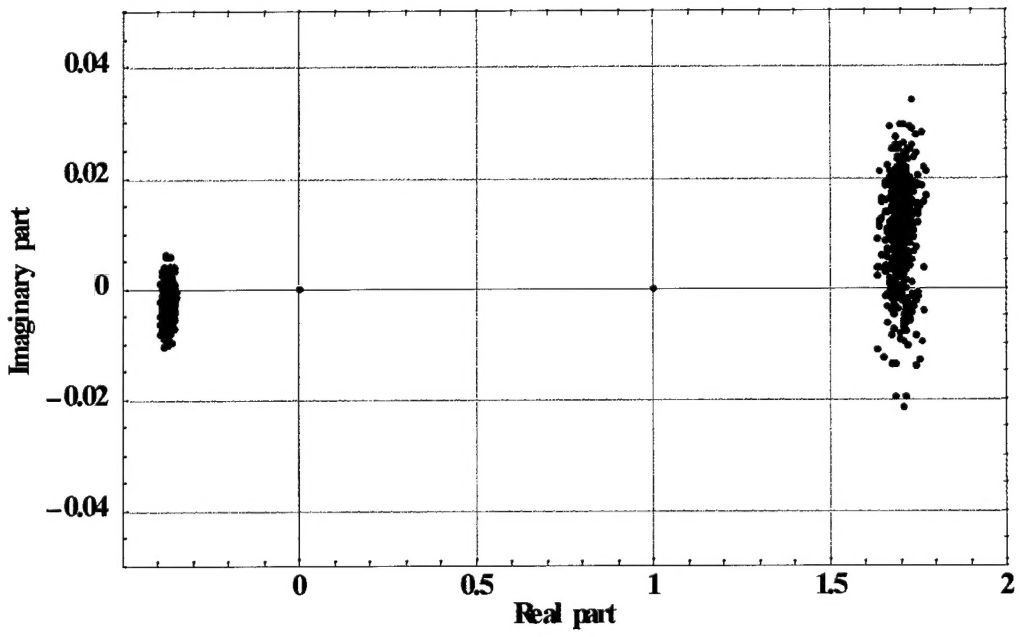

Figure D8: Dispersion of the normalized reflection coefficient (Blue) and the refractive index (red) for a microscope slide.